Appendix K Parameter improvement for dry and wet compaction of crushed salt

Table of content

1 Objective and scope

In order to investigate whether the material models for crushed salt implemented in CODE_BRIGHT are in principle applicable for simulating the long-term compaction behaviour in lab, a simplified model was developed, and several model variants, following the execution of the stress-controlled long-term compaction test (see chapter 2.4.2 and Appendix E) under dry conditions at ambient and elevated temperature, and with brine inflow were simulated.

The objective of these simulations was to test the capabilities of the implemented models, especially with coupling of mechanical, hydraulic and thermal effects, in a simple system. The material parameters that were used for back-calculation of the experiment are coming from different reports:

- GRS-254: initial parameters from Repoperm project phase 1,

- GRS-288: a further developed data set used for the Preliminary Safety Analysis of the Gorleben site (VSG)

The calculation results were compared to the experimental findings and selective material parameter were fitted if necessary. The adapted material parameters are shown in the figures, renamed by GRS (2016).

2 Model description

2.1 Geometrical model

For the simulation of the crushed salt sample an axial-symmetric model of 110 mm height and 120 mm diameter was used. In addition, the steel piston is $h_0 = 340$ mm in height and in diameter equal to the sample size. The axial load is applied on top of the steel piston. (Fig. 2.1).

The initial temperature of both, the steel cylinder and the crushed salt sample is about 29 °C. The initial porosity of the steel piston is 0.1 % and the porosity of the crushed salt is 27.536 %. The initial stress σ_y is about 1 MPa.

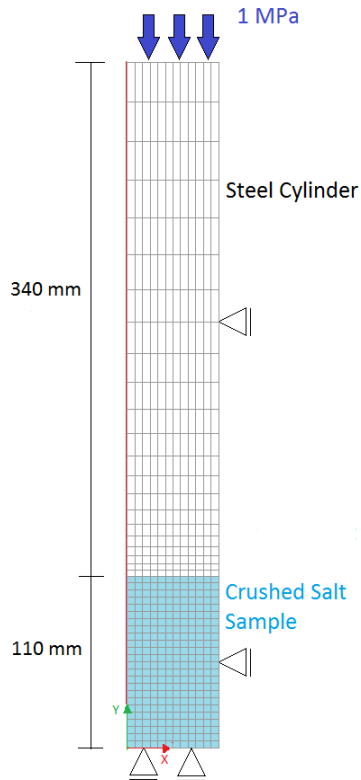**Fig. 2.1**   Overview of the model geometry

2.2   Physical model and constitutive laws

The model for mechanical behaviour of the crushed salt includes the following mechanisms:

- elastic deformation

- dislocation creep

- viscoplasticity for granular material representing grain reorganisation and breaking

- fluid assisted diffusional transfer

- thermal expansion (for non-isothermal simulations)

The various contributions are combined by adding the individual deformation rates. A description of the formulations is given further down.

Heat transfer is restricted to conductive flux of heat in the non-isothermal simulation. For thermal-mechanical coupling linear thermal expansion of solid and liquid phases is considered.

In the following sections, the constitutive laws applied are described.

2.2.1 Mechanical behaviour

In CODE_BRIGHT the deformation ratio is calculated as the sum of different contributions:

$$\dot{\varepsilon}_{CS} = \dot{\varepsilon}^{EL} + \dot{\varepsilon}^{DC} + \dot{\varepsilon}^{VP} + \dot{\varepsilon}^{FADT} + \dot{\varepsilon}^{TH} \tag{1}$$

(EL = linear elasticity, DC = dislocation creep, VP = viscoplasticity for granular materials, FADT = fluid assisted diffusional transfer, TH = thermal influence) /COD 10/. The individual contributions are explained in the following sections.

2.2.1.1 Linear elasticity

This law describes the elastic behaviour of the material. An isotropic approach is chosen because a statistic orientation of the grains is assumed. Following Hooke´s law, in CODE_BRIGHT linear elasticity is described using two independent variables, Young's modulus E and Poisson´s ratio ν. Young's modulus shows a linear dependence on porosity according to

$$E = E_0 + (\eta - \eta_0)\frac{dE}{d\eta} \tag{2}$$

(E = Young's modulus, dE/dη = variation of Young's modulus with porosity, η_0 = reference porosity). η_0 and E_0 are given constants /COD 10/.

2.2.1.2   Dislocation creep

This law describes the dislocation creep which is a time dependent deformation mechanism. CODE_BRIGHT uses a modification which enables a creep compaction for materials with a significant porosity /COD 10/. For stationary conditions the equation is

$$\dot{\varepsilon}_{ij}^{DC} = \frac{1}{\mu_{dev}^{DC}} \cdot \Phi(F) \cdot \frac{\partial G}{\partial \sigma'} \tag{3}$$

$\Phi(F) = F^n$ is a scalar function with n = stress exponent, F = function of stress and G = flow rule.

The flow rule and the function of stress are defined as

$$G = F = \sqrt{q^2 + \left(\frac{-p'}{\alpha_p}\right)^2} \tag{4}$$

Here q is the deviatoric stress and p' is the mean normal stress. α_p is a material parameter and defined as

$$\alpha_p = \left(\frac{\mu_{vol}^{DC}}{\mu_{dev}^{DC}}\right)^{1/(n+1)} \tag{5}$$

μ_{dev} is the deviatoric viscosity, μ_{vol} is the volumetric viscosity and both are dependent on the void ratio e:

$$\frac{1}{\mu_{dev}^{DC}} = A(T) \cdot g_{dev}^{DC}(e) \qquad \frac{1}{\mu_{vol}^{DC}} = A(T) \cdot g_{vol}^{DC}(e) \tag{6) + (7}$$

The dependence on temperature is described by the structural parameter A_A, the activation energy Q_B, the general gas constant R and the absolute temperature T:

$$A(T) = A_A \cdot \exp(\frac{-Q_A}{R \cdot T}) \tag{8}$$

The functions of the void ratio are described by

$$g_{vol}^{DC}(e) = 3 \cdot (g-1)^n \cdot f \tag{9}$$

$$g_{dev}^{DC}(e) = \left(\sqrt{\frac{1+g+g^2}{3}}\right)^{n-1} \cdot \left(\frac{2 \cdot g + 1}{3}\right) \cdot f + \frac{1}{\sqrt{g}} \tag{10}$$

where g and f are given by

$$g = \frac{1}{(1-f)^2} \qquad f = \sqrt{\frac{2e}{3 \cdot (1-e^{3/2}) \cdot (1+e)}} \tag{11) + (12}$$

2.2.1.3   Viscoplasticity for granular materials

This is a general model for soils to describe the viscoplasticity and the plastic behaviour of the bond between the grains:

$$\dot{\varepsilon}_{ij}^{VP} = \Gamma \cdot <\Phi(F)> \frac{\partial G}{\partial \sigma} \tag{13}$$

where $\Phi(F) = F^m$ for F > 0 otherwise $\Phi(F) = 0$ (14)

The flow rule and the yield function for crushed salt are defined by

$$G = F = q^2 - \delta^2 (p_0 \cdot p' - p'^2) \tag{15}$$

with the deviatoric stress q, the mean normal stress p' and a parameter δ.

The temperature-dependent viscosity is given by

$$\Gamma = \Gamma_0 \cdot \exp(\frac{-Q}{R \cdot T}) \tag{16}$$

Here Γ_0 is a scaling factor, Q is the activation energy, R is the gas constant and T is the temperature.

Strain hardening of the material is achieved by a change of the pressure p_0 with the volumetric deformation ε_V. D and l are parameters.

$$dp_0 = D \cdot l \cdot \varepsilon_V^{l-1} \cdot d\varepsilon_V \tag{17}$$

The formulation G = F does not permit a volume increase. This restriction is acceptable for the description of crushed salt.

2.2.1.4 Viscoelasticity for Saline Materials (FADT)

The deformation mechanism fluid assisted diffusional transfer (FADT) was introduced to describe the influence of liquid on deformation behaviour. The deformation rate is linear and stress dependent:

$$\dot{\varepsilon}_{ij}^{FADT} = \frac{1}{2\mu_{dev}^{FADT}}(\sigma'_{ij} - p' \cdot \delta_{ij}) + \frac{1}{3\mu_{vol}^{FADT}} p' \cdot \delta_{ij} \tag{18}$$

μ_{dev} is the deviatoric viscosity, μ_{vol} is the volumetric viscosity and δ_{ij} is the Kronecker symbol.

The volumetric viscosity and the deviatoric viscosity are described by

$$\frac{1}{\mu_{vol}^{FADT}} = \frac{16B(T)\sqrt{S_l}}{d_0^3} g_{vol}^{FADT}(e) \qquad \frac{1}{2\mu_{dev}^{FADT}} = \frac{16B(T)\sqrt{S_l}}{d_0^3} g_{dev}^{FADT}(e) \tag{19) + (20}$$

The viscosities are dependent on the degree of saturation (S_l), the grain size (d_0) and functions of temperature and void ratio.

$$B(T) = \frac{A_B}{R \cdot T} \cdot \exp(\frac{Q_B}{R \cdot T}) \tag{21}$$

captures the dependence on the temperature and contains the pre-exponential parameter A_B, the activation energy Q_B, the general gas constant R and the temperature T.

$$g_{vol}^{FADT}(e) = \frac{3g^2 \cdot e^{3/2}}{1+e} \quad \text{and} \quad g_{dev}^{FADT}(e) = \frac{g^2}{1+e}$$

(22) + (23)

capture the dependence on the void ratio e. The functions g and f are defined as in equation (11) and (12).

2.2.1.5 Thermal expansion

Thermal expansion is described by

$$\dot{\varepsilon}ij^{TH} = 3b_S \Delta T$$

(24)

(b_s = Linear thermal expansion coefficient of the material)

2.2.2 Thermal behaviour

Heat transfer is restricted to conductive flux of heat following Fourier's law. Thermal conductivity is dependent on conductivities of the dry material and of the pore fluids, and on porosity. The effective thermal conductivity is calculated as the geometric weighted mean for the dry or the saturated case:

$$\lambda_{dry} = \lambda_{solid}^{(1-\phi)} \cdot \lambda_{gas}^{\phi} \qquad \lambda_{sat} = \lambda_{solid}^{(1-\phi)} \cdot \lambda_{liq}^{\phi}$$

(31) + (32)

The thermal conductivity of the solid salt fraction is dependent on temperature. This is approximated by a polynomial:

$$\lambda_{solid} = (\lambda_{solid})_0 + a_1 T + a_2 T^2 + a_3 T^3$$

(33)

In the drift simulation, however, thermal conductivity of air or water in the pore space was neglected, so that only the solid thermal conductivity contributed to heat transfer.

2.3 Material data

2.3.1 Crushed salt, GRS-254

Elastic deformation behaviour

E_0	1.00	MPa
η_0	0.30	-
E_0/η_0	-4.50E+03	MPa
v	0.27	-

Dislocation creep

A_A	2.08E-06	$s^{-1}MPa^{-n}$
Q_A	5.40E+04	$J\ mol^{-1}$
n	5.00	-

Viscoplastic deformation behaviour

δ	10.00	-
Γ_0	7.00E-04	s^{-1}
Q	5.40E+04	$J\ mol^{-1}$
p_0	0.10	MPa
D	1.00E+05	MPa
l	4.00	-

Linear behaviour under temperature

b_s	4.20E-05	$°C^{-1}$

Fluid assisted diffusional transfer

d_0	1.50E-04	m
A_B	1.00E-14	$s^{-1}\ MPa^{-1}\ m^3$
Q_B	24530	$J\ mol^{-1}$

2.3.2 Crushed salt, GRS-288

Elastic deformation behaviour

E_0	1.00	MPa
η_0	0.30	-
E_0/η_0	-4.50E+03	MPa
v	0.27	-

Dislocation creep

A_A	2.08E-06	$s^{-1}MPa^{-n}$

Q_A	5.40E+04	J mol^{-1}
n	5.00	-

Viscoplastic deformation behaviour

δ	10.00	-
Γ_0	7.00E-04	s^{-1}
Q	5.40E+04	J mol^{-1}
p_0	0.10	MPa
D	1.00E+05	MPa
l	4.00	-

Linear behaviour under temperature

b_s	4.20E-05	°C^{-1}

Fluid assisted diffusional transfer

d_0	1.50E-04	m
A_B	1.00E-14	s^{-1} MPa^{-1} m^3
Q_B	24530	J mol^{-1}

2.4 Simulation variants, schedule, and boundary conditions

First, a model for dry compaction was calibrated. The resulting material parameters were then used as input for a numerical simulation of a compaction test with wet material. This allowed for the first time to estimate the parameters for the fluid assisted diffusional transfer (FADT) on the basis of a real test. This is significant as the FADT is believed to describe the impact of water or brine on compaction.

Though it is a thermal-hydraulic-mechanical (THM) problem, the modelling was graduated into three phases.

- The first phase from interval 1 to interval 8 is the mechanical phase. Here the stress is increased stepwise.
- The second phase from interval 9 to interval 14 is the thermal-mechanical phase. The temperature first increases up to 55 °C. Then, after some days the temperature decreases again to 34 °C while the stress level is kept constant.
- The last phase is the thermal-hydraulic-mechanical phase. In interval 15, when the experiment is flooded with brine, the fluid assisted diffusional transfer (FADT) model is active.
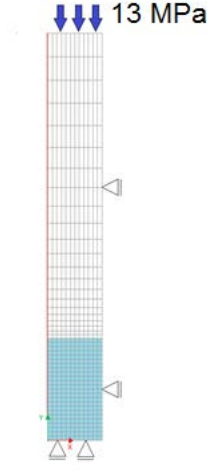
11

The time interval representing the calculation time of CODE_BRIGHT, starting at 0 days, though the laboratory experiment is still running since 50 days. Due to the fact, that the model is not capable to simulate the man made pre-consolidation process, the stress level after 50 days is taken as initial condition for the calculation process. Hence t = 0 days in modelling is equal to t =50 days in the laboratory experiment.
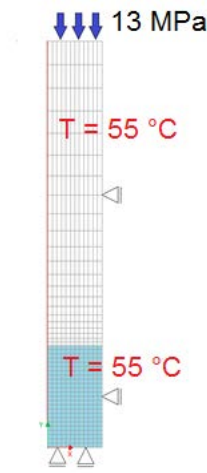
In the following, the initial and boundary conditions of the simulation cases are discussed in detail.
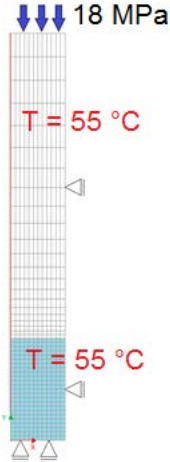
Interval 1 and 2	0 – 81 days (calculation) or rather 50 – 131 days (lab testing)
Interval 1 and 2	The simulation started by rising up the vertical stress to 4 MPa in Interval 1 (0.0 – 0.1 days). In Interval 2 (0.1 – 81.0 days) the stress is kept constant.
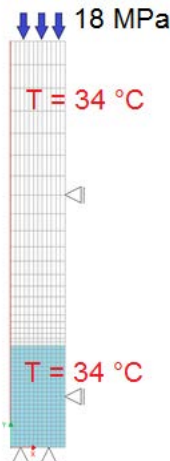
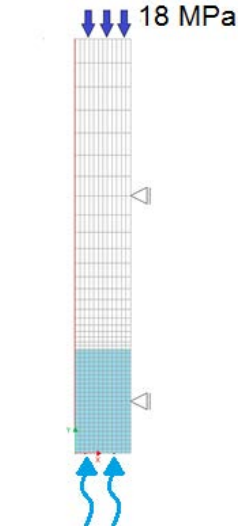|	
Interval 3 and 4	81 – 217 days (calculation) or rather 131 – 267 days (lab testing)
Interval 3 and 4	In Interval 3 (81 – 81.1 days) the stress increased to 7 MPa. In interval 4 (81.1 – 217.0 days) the stress is kept constant.

Interval 5 and 6	217 – 307 days (calculation) or rather 267 – 357 days (lab testing)
Interval 5 and 6	In interval 5 (217.0 – 217.1 days) the stress increased to 10 MPa. In interval 6 (217.1 days – 307.0 days) it is kept constant.

Interval 7 and 8	307 – 460 days (calculation) or rather 357 – 510 days (lab testing)
Interval 7 and 8	In interval 7 (307.0 – 307.1 days) the stress increased to 13 MPa and kept constant in interval 8 (307.1 – 460.0 days). After 460 days the pure mechanical phase is finished.

Interval 9 and 10	460 – 768 days (calculation) or rather 510 – 818 days (lab testing)
Interval 9 and 10	In interval 9 (460.0 – 461.0 days) the thermal-mechanical phase begins. The temperature increased to 55°C in the steel cylinder and in the crushed salt. Then the temperature is kept konstant in interval 10 (461.0 – 768.0 days).

Interval 11 and 12	768 – 800 days (calculation) or rather 818 – 850 days (lab testing)
Interval 11 and 12	In interval 11 (768.0 – 769.0 days) the last loading increment increased the stress up to a value of 18 MPa, while the temperature is kept constant at 55 °C.

Interval 13 and 14	800 – 1128 days (calculation) or rather 850 – 1178 days (lab testing)
Interval 13 and 14	In interval 13 (800.0 – 801.0 days) the sample and the steel cylinder are cooled down to 34°C. The stress is kept constant.

Interval 15	1128 – 1524 days (calculation) or rather 1178 – 1574 days (lab testing)
18 MPa **Interval 15**	In interval 15 the inflow of brine is simulated by activation of the fluid assisted diffusional transfer model.

3 Back calculation

3.1 Back calculation using data set from the first RepoPerm project phase

The first calculation results using the data set from the first RepoPerm project phase are shown in Fig. 3.1 and compared to the experimental findings (lower limit of porosity evolution). During the mechanical phase and prior to the increase of the temperature the calculation results follow the trend of the measurements. During the thermal phase the calculation results highly overestimate the compaction process. When the sample is flooded, the FADT parameter is not able to simulate the sudden decrease of porosity.
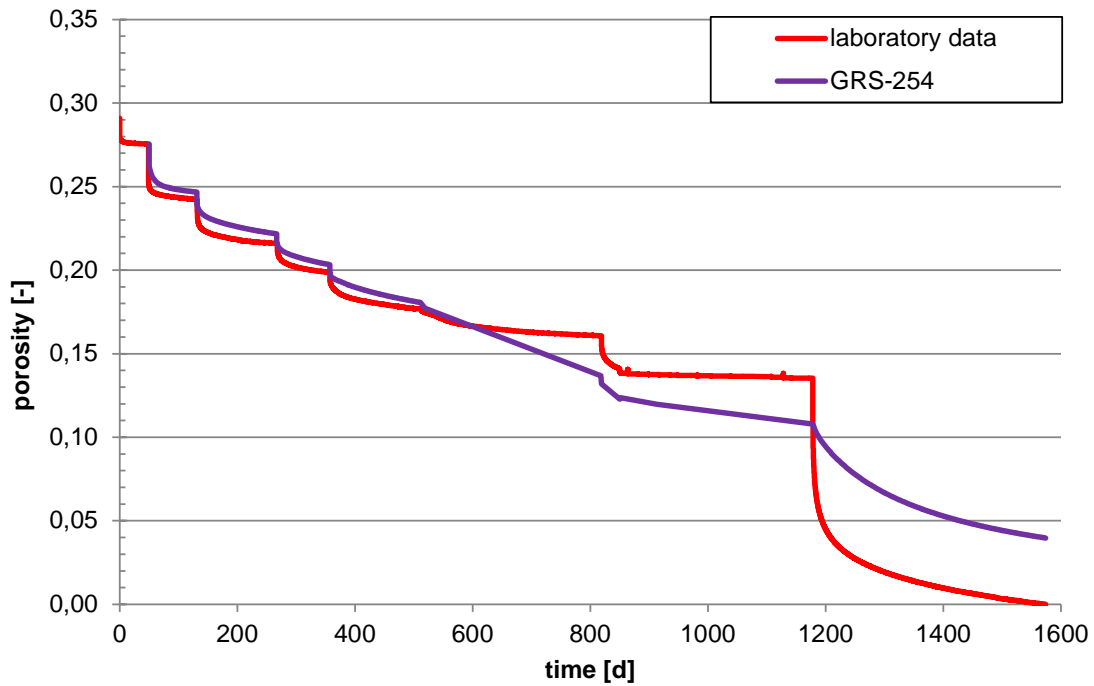
Fig. 3.1   Porosity evolution with time, parameter from GRS-254

3.2   Back calculation using data set from the preliminary Safety Analysis of the Gorleben site

For the simulation work that was done within the project phase for the preliminary Safety Analysis of the Gorleben site, few parameters were changed to get an approximated curve, Fig. 3.2. The measurements during the mechanical phase were only available for parameter improvement. Therefore the decrease of porosity is very well captured by the modelling results, although the compaction process at elevated temperatures is still overestimated.
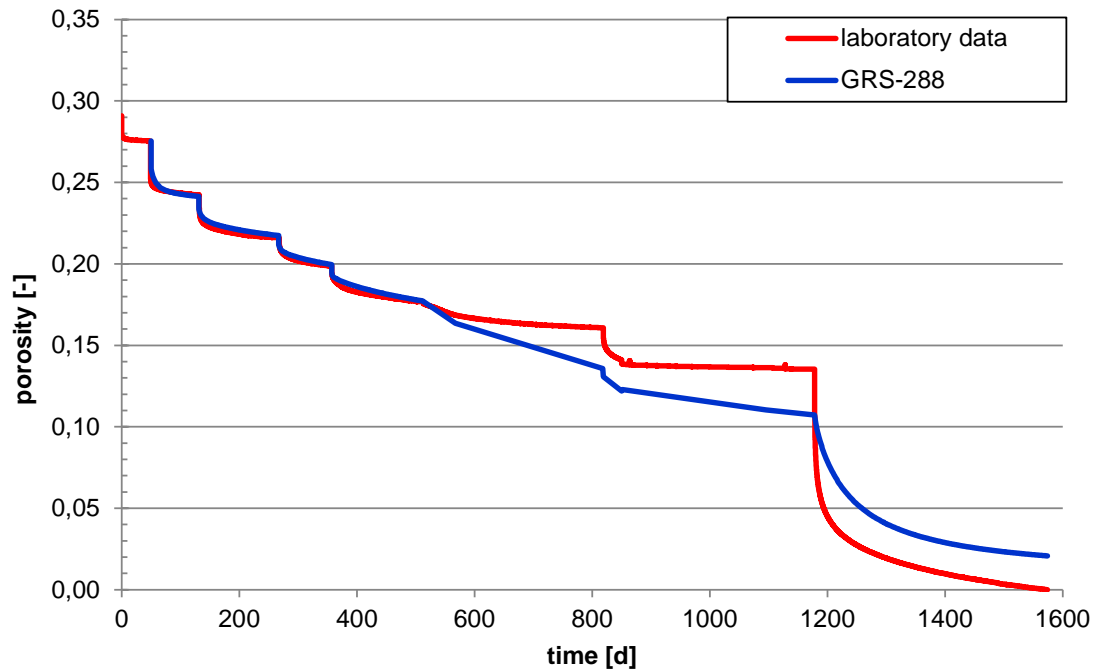
Fig. 3.2   Porosity evolution with time, parameter from GRS-288

3.3   Parameter identification

3.3.1   Methodical approach

In order to investigate whether the material models for crushed salt implemented in CODE_BRIGHT are in principle applicable for simulating the long-term compaction behaviour in lab, a simplified model was developed, and several model variants, following the execution of the stress-controlled long-term compaction test (see chapter 2.4.2 and Appendix E) under dry conditions at ambient and elevated temperature, and with brine inflow were simulated.

The objective of these simulations was to test the capabilities of the implemented models, especially with coupling of mechanical, hydraulic and thermal effects, in a simple system. The material parameters that were used for back-calculation of the experiment are referenced to the individual GRS report numbers:

- GRS-254: initial parameters from Repoperm project phase 1,

- GRS-288: a further developed data set used for the Preliminary Safety Analysis of the Gorleben site (VSG)

The calculation results were compared to the experimental findings and selective material parameter were fitted if necessary. The adapted material parameters are shown in the figures, renamed by GRS (2016).

First, a model for dry compaction was calibrated. The resulting material parameters were then used as input for a numerical simulation of a compaction test with wet material. This allowed for the first time to estimate the parameters for the fluid assisted diffusional transfer (FADT) on the basis of a real test. This is significant as the FADT is believed to describe the impact of water or brine on compaction.

Though it is a thermal-hydraulic-mechanical (THM) problem, the modelling was graduated into three phases.

- The first phase from interval 1 to interval 8 is the mechanical phase. Here the stress is increased stepwise.
- The second phase from interval 9 to interval 14 is the thermal-mechanical phase. The temperature first increases up to 55 °C. Then, after some days the temperature decreases again to 34 °C while the stress level is kept constant.
- The last phase is the thermal-hydraulic-mechanical phase. In interval 15, when the experiment is flooded with brine, the fluid assisted diffusional transfer (FADT) model is active.

The time interval representing the calculation time of CODE_BRIGHT, starting at 0 days, though the laboratory experiment is still running since 50 days. Due to the fact, that the model is not capable to simulate the man made pre-consolidation process, the stress level after 50 days is taken as initial condition for the calculation process. Hence t = 0 days in modelling is equal to t =50 days in the laboratory experiment.

3.3.2   Parameter variation mechanical phase

In the mechanical phase the following laws were used:

- Linear Elasticity
- Viscoplasticity for Saline Materials (Dislocation Creep)
- Viscoplasticity for Granular Materials (Viscoplasticity).

It was decided to vary minimum one parameter in every law to get an adequate overview.

Remember the modelled mechanical phase starts at 50 days and ends at 510 days.

3.3.2.1 Viscoplasticity

The parameter of GRS-254 were the basis for this calculation.

The input parameters are:
- m = stress power
- Γ_0 = viscosity
- Q = activation energy
- D = constant in hardening law
- p_0 = initial value of p_0
- l = power of hardening law

The parameter D, I and Γ_0 were modified. The next figures show the influence on parameter variation.

<u>Variation of the constant D</u>

The initial value was D = 1.00E+05 MPa. At first the parameter was decreased to D = 1.00E+04 MPa. The calculation results overestimated the compaction process at axial stress of 13 MPa. When the parameter was increased to D = 1.00E+06 MPa the compaction process is highly underestimated. Therefore, constant D should be less than 1.00E+05 MPa.
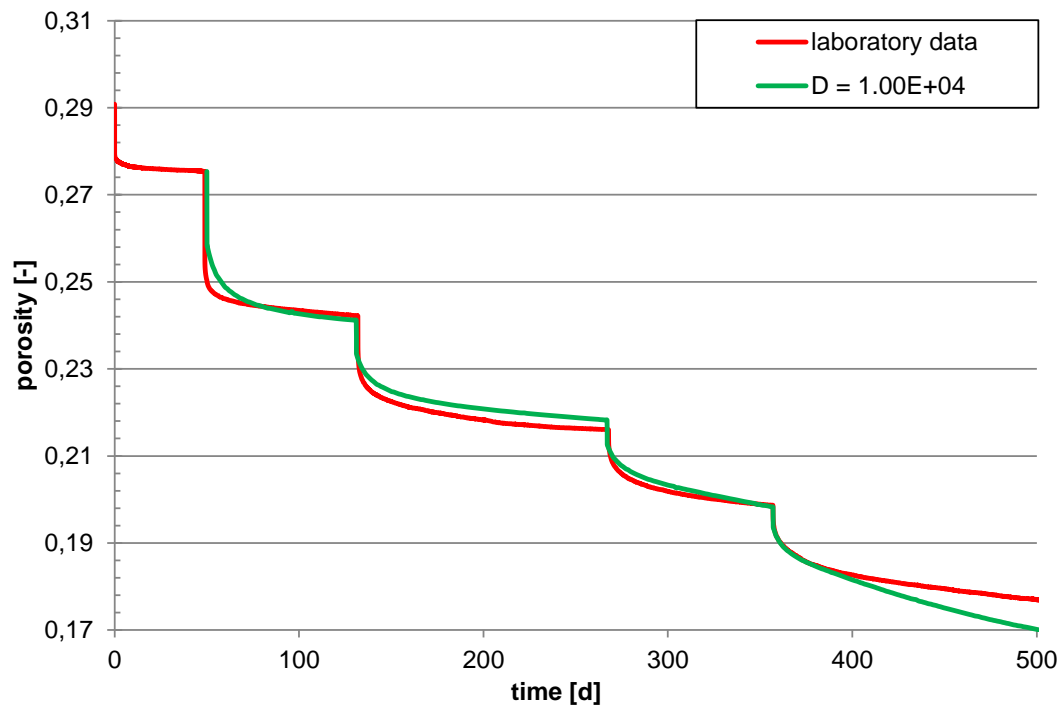
Fig. 3.3   Porosity evolution with time, variation **D=1.00E+04 MPa**
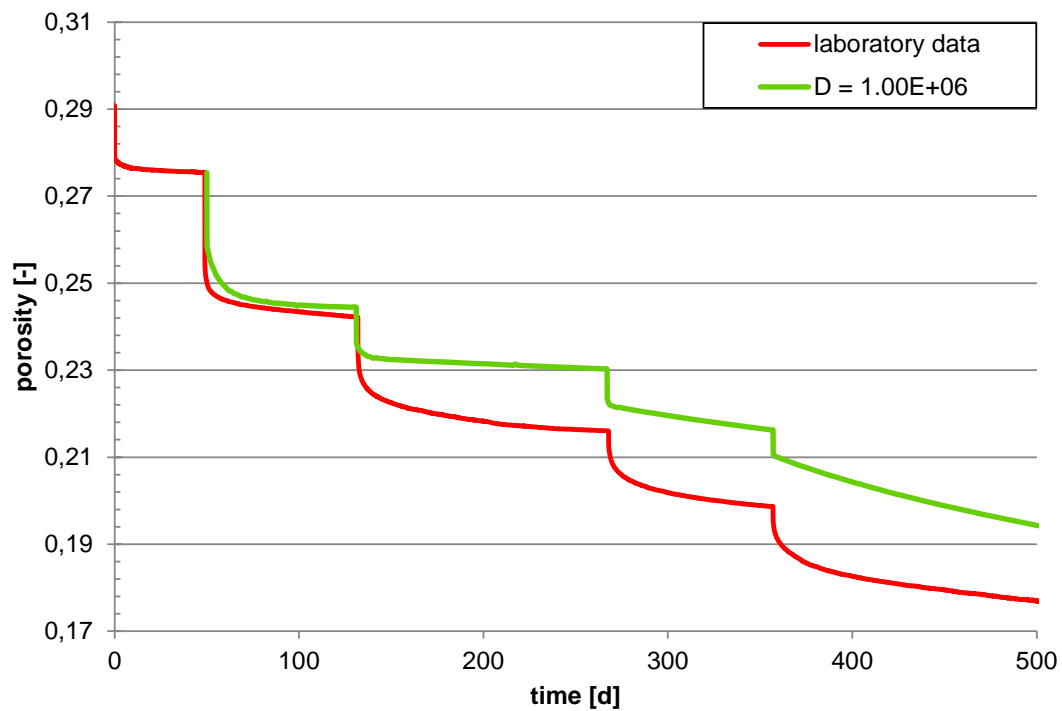

Fig. 3.4   Porosity evolution with time, variation **D=1.00E+06 MPa**

<u>Variation of the power of the hardening law l</u>

The initial value was l = 4.00 [-]. To see how the parameter effects the graph the variations to l = 0.4 and l = 40 were chosen.
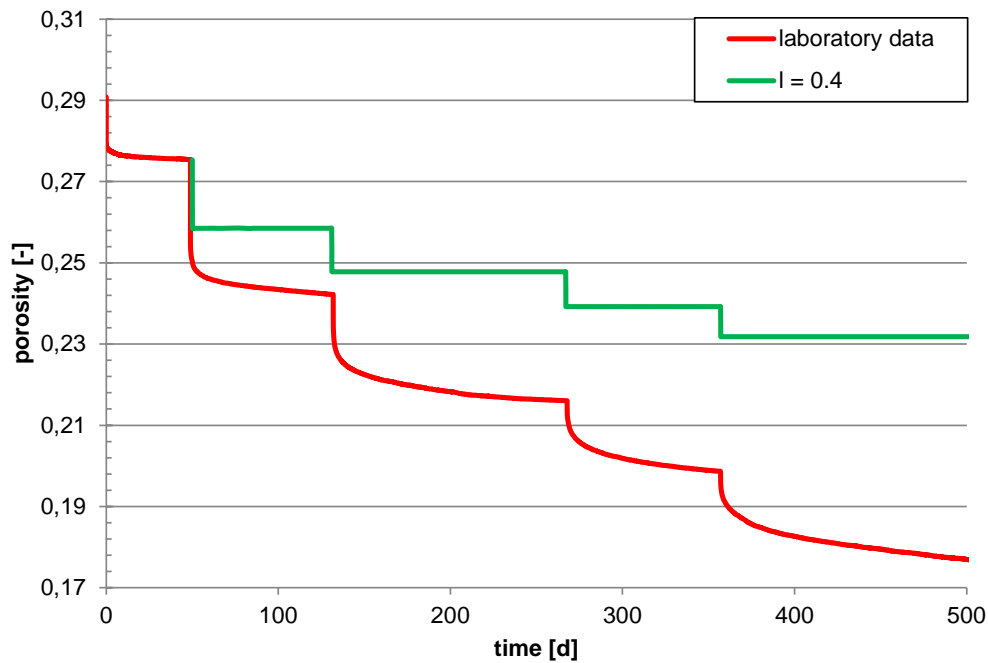

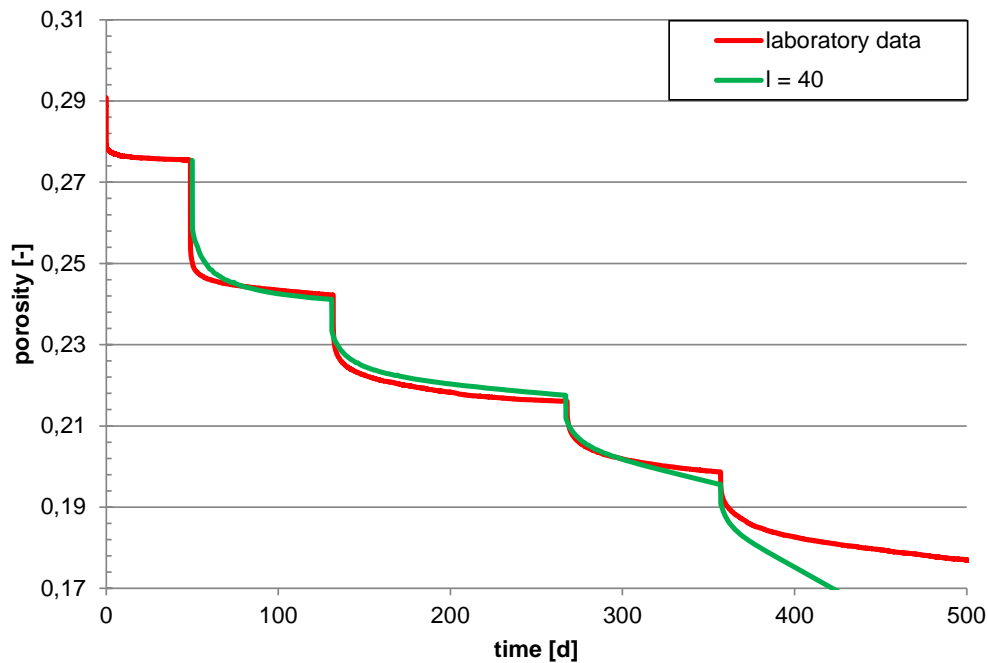**Fig. 3.5**   Porosity evolution with time, variation **l=0.4 MPa**

Fig. 3.6   Porosity evolution with time, variation **l=40 MPa**

<u>Variation of the viscosity</u>

The initial value of the viscosity was $\Gamma_0 = 7.00E-04\ s^{-1}$.
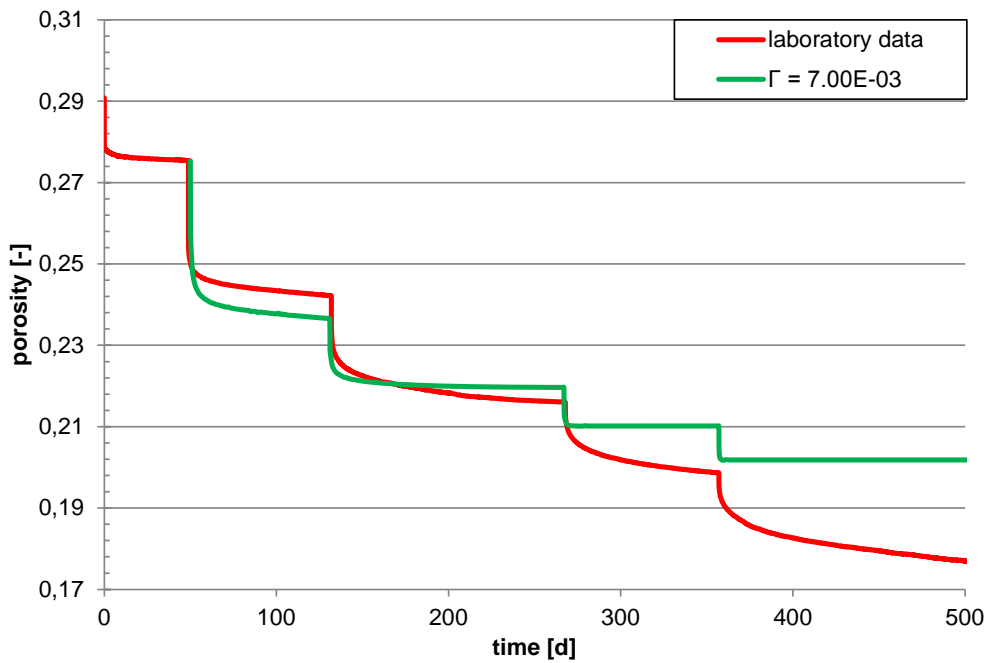
Fig. 3.7   Porosity evolution with time, variation $\mathbf{\Gamma_0=7.00E-03\ s^{-1}}$
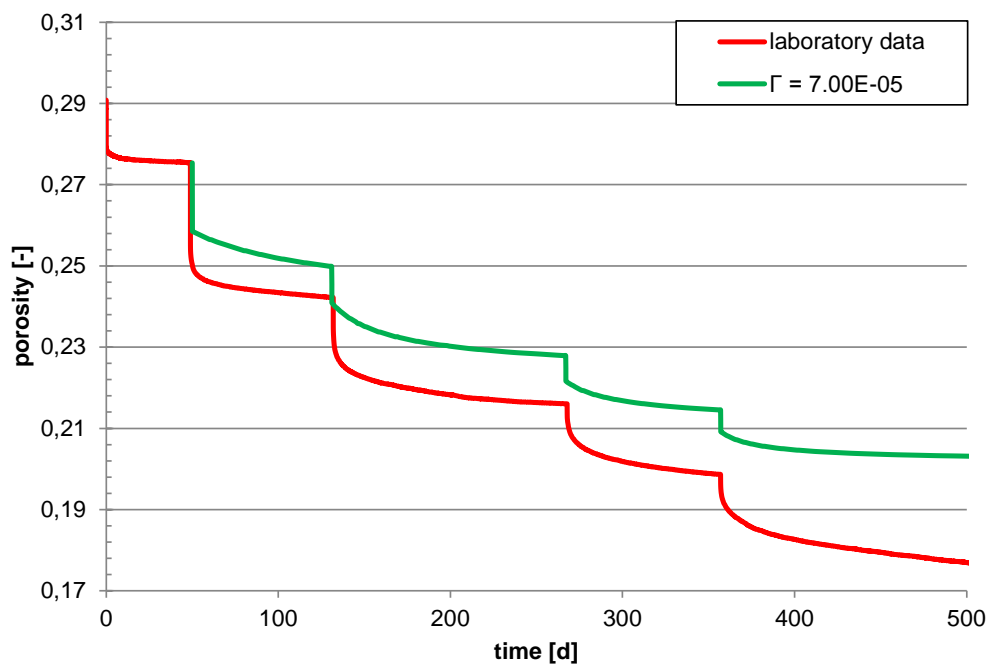
Fig. 3.8   Porosity evolution with time, variation $\mathbf{\Gamma_0=7.00E-05\ s^{-1}}$

<u>Variation of constant D and viscosity Γ_0</u>

After vary the parameter separately two parameter should be varied together. Judging by the pictures the decision was to vary the constant D together with the viscosity Γ_0. So D = 1.00E+04 MPa and Γ_0 = 7.00E-05 s^{-1} were chosen to put in one modelling.
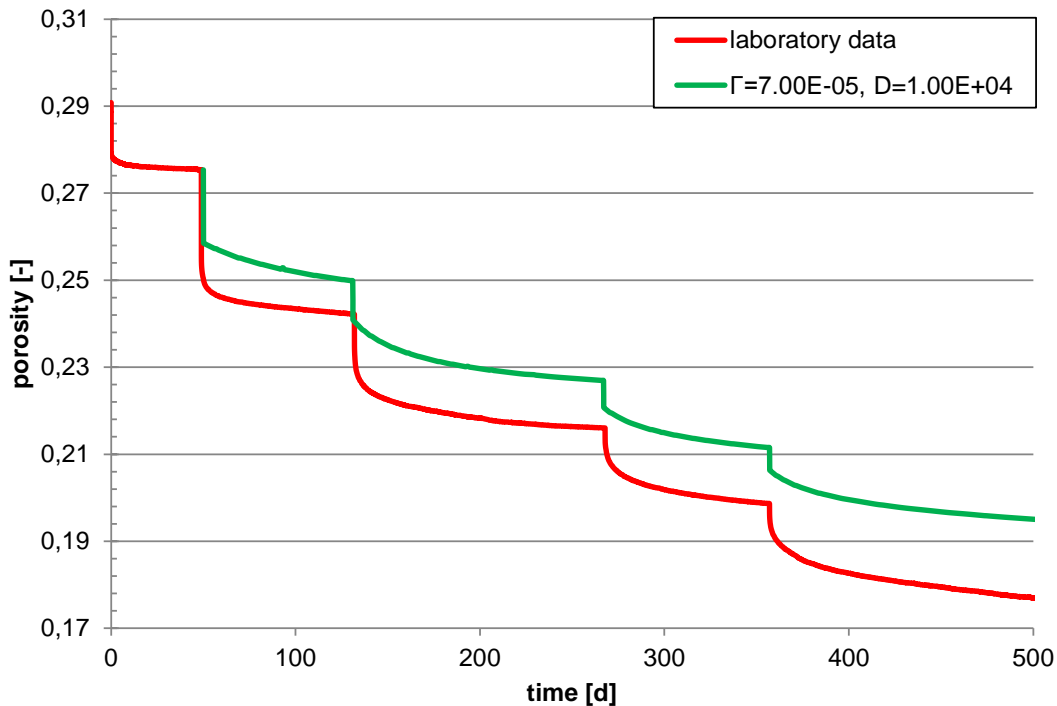

Fig. 3.9   Porosity evolution with time, variation **Γ_0=7.00E-05 s^{-1}** and **D=1.00E+04 MPa**

The parameters were adopted to use it for the next variations.

3.3.2.2   Dislocation creep

In this change the parameter chosen in the viscoplasticity variation were assumed (D=1.00E+04 MPa and Γ_0=7.00E-05 s^{-1}). The residual parameters are the same out of the GRS-254 material table.

Possible parameters for variation were:
- A_A = pre-exponential parameter
- Q_A = activation energy
- N = stress power

The decision was to vary the pre-exponential parameter. Its initial value was $A_A = 2.08\text{E-06}$ $\text{s}^{-1}\text{MPa}^{-n}$. The first variations of this parameter were $A_A = 2.08\text{E-05}$ $\text{s}^{-1}\text{MPa}^{-n}$ and $A_A = 2.08\text{E-07}$ $\text{s}^{-1}\text{MPa}^{-n}$.
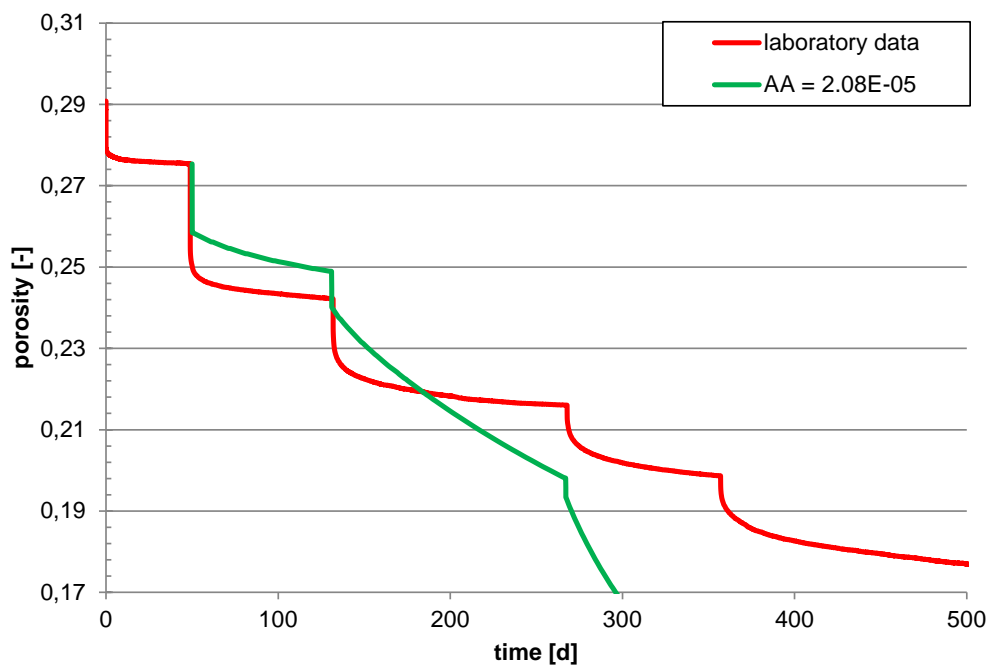

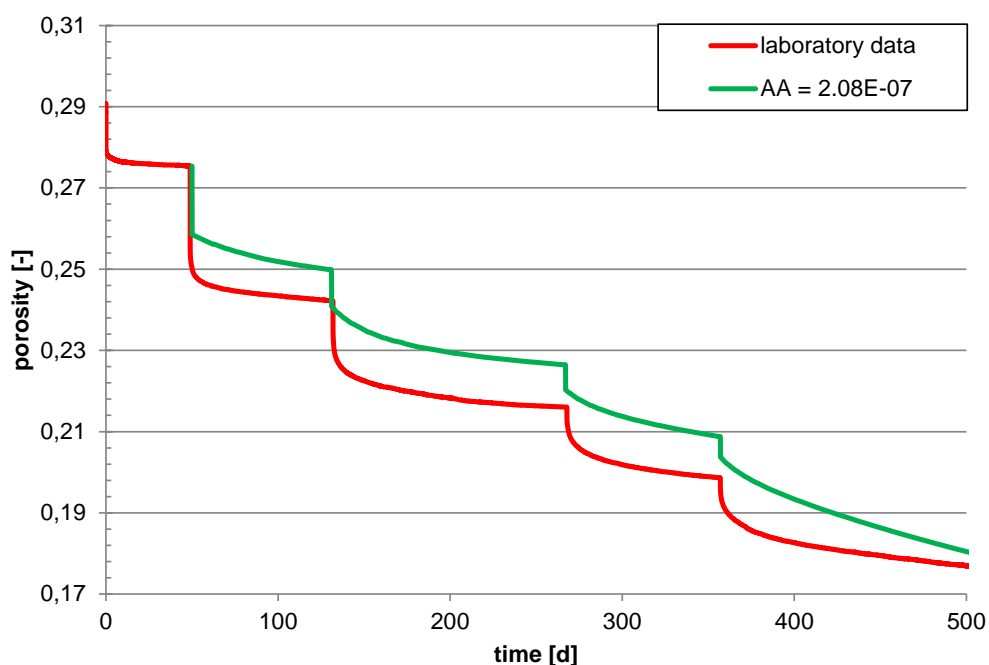**Fig. 3.10**   Porosity evolution with time, variation $A_A=2.08\text{E-05}$ $\text{s}^{-1}\text{MPa}^{-n}$

Fig. 3.11   Porosity evolution with time, variation $A_A=2.08\text{E-07}$ $\text{s}^{-1}\text{MPa}^{-n}$

This graph looks more convenient than the other one, but still not perfect. So the pre-exponential parameter will be reduced to A_A = 2.08E-08 $s^{-1}MPa^{-n}$.
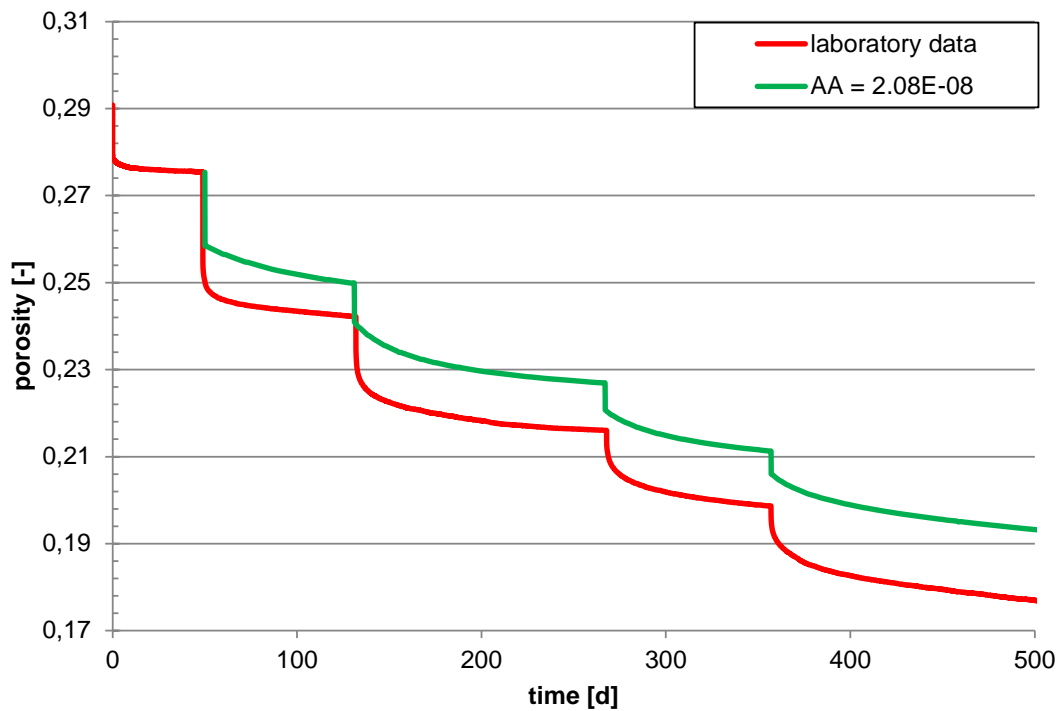

Fig. 3.12   Porosity evolution with time, variation $\mathbf{A_A=2.08E\text{-}08\ s^{-1}MPa^{-n}}$

Parameter A_A = 2.08E-08 $s^{-1}MPa^{-n}$ will be adopted for the next variations.

3.3.2.3   Linear Elasticity

The linear elasticity will be used to eliminate the steps between the modelled graph and the measured graph. From the prevenient variations this parameters were adopted: D=1.00E+04 MPa, Γ_0=7.00E-05 s^{-1} and A_A = 2.08E-08 $s^{-1}MPa^{-n}$.

Possible parameters for variation were:
- E = Young Modulus
- $dE/d\Phi$ = Variation of Young Modulus with porosity
- v = Poisson´s Ratio
- Φ_0 = Reference porosity
- Φ_{min} = Minimum porosity
- E_{min} = Minimum elastic modulus

26

The decision was to vary $dE/d\Phi$ and Φ_0.

Modification of the Variation of Young Modulus with porosity $dE/d\Phi$

The initial value was - 4.50E+03 MPa. Because of the big steps the first variation was $dE/d\Phi$ = - 3.50E+03 MPa.
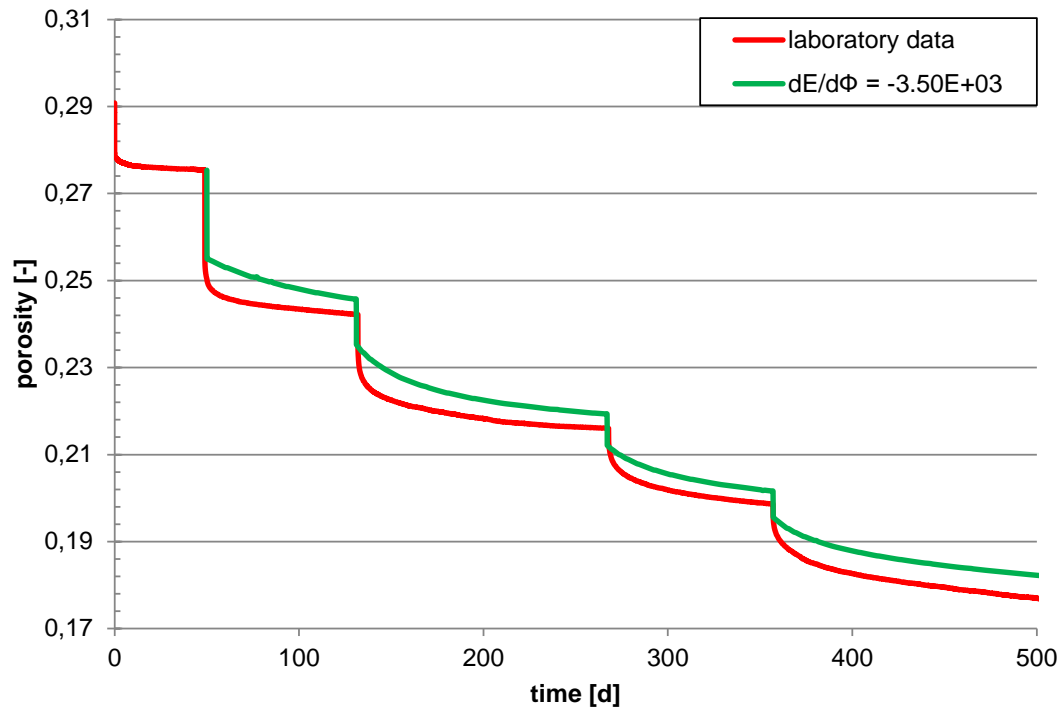

Fig. 3.13   Porosity evolution with time, variation **dE/dΦ=- 3.50E+03 MPa**

The steps are smaller but the graph is even not satisfying. So the variation of the Young Modulus with the porosity was set to - 3.00E+03 MPa.
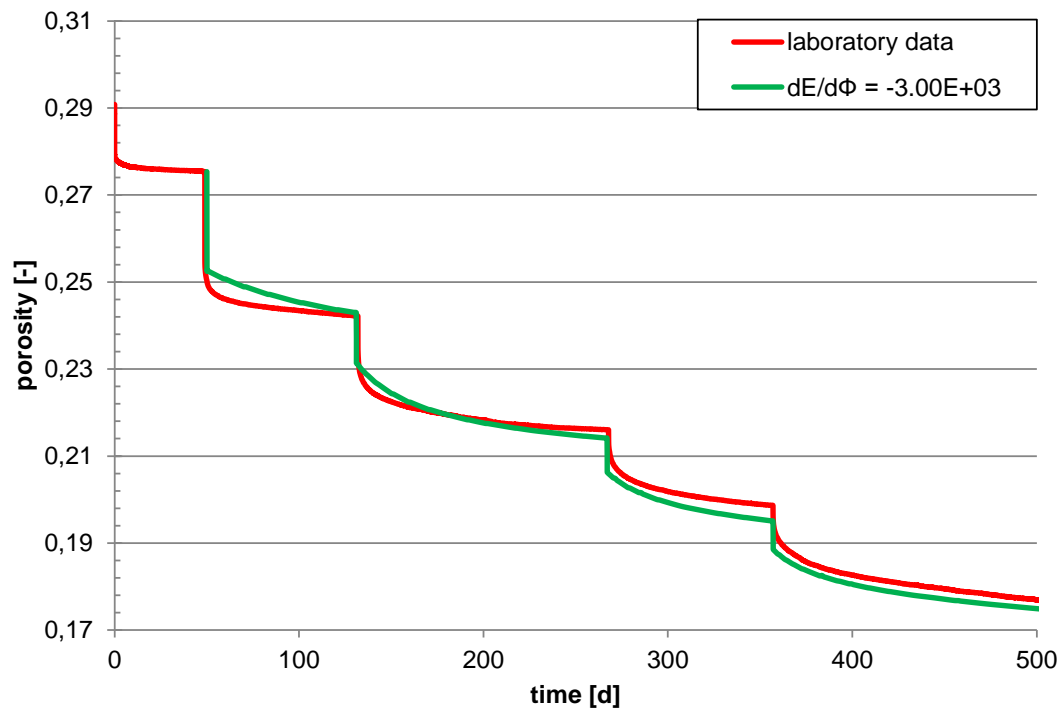
Fig. 3.14   Porosity evolution with time, variation **dE/dΦ=- 3.00E+03 MPa**

The graph underestimates the porosity in the beginning and overestimates it in the end. To get a better approximation dE/dΦ = - 3.20E+03 MPa was chosen.
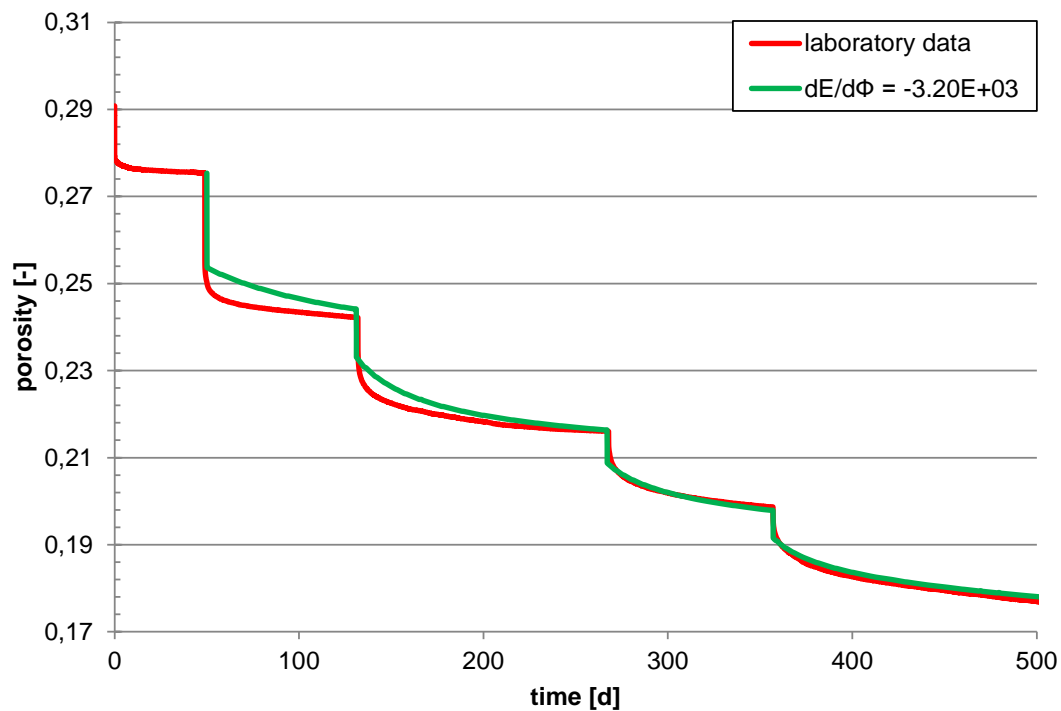

Fig. 3.15   Porosity evolution with time, variation **dE/dΦ=-3.20E+03 MPa**

At the time of 250 days the curve is pretty good approached to the measured graph. To get this result also in the beginning the reference porosity should be varied.

Variation of the reference porosity Φ_0

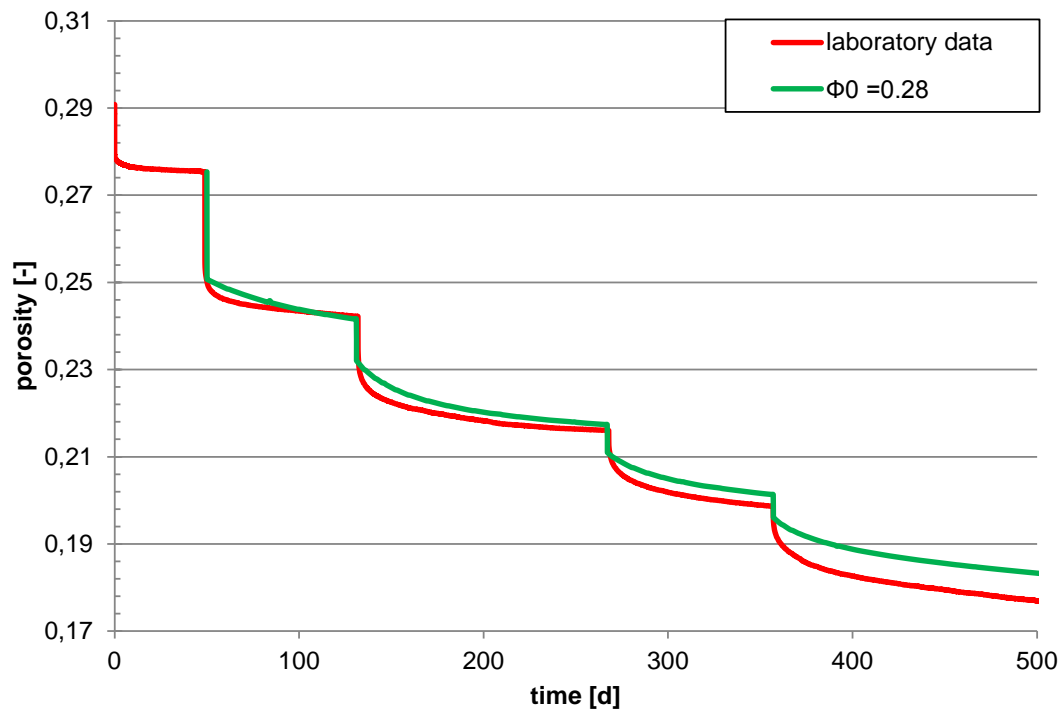The initial value of the reference porosity was 30 %. First the reference porosity was reduced to 28 %.

Fig. 3.16   Porosity evolution with time, variation **of Φ0=0.28**

The graph looks very good. Now the expectation was that a combination of dE/dΦ = 3.20E+03 MPa and Φ_0 = 28 % will make the good approximated graph.
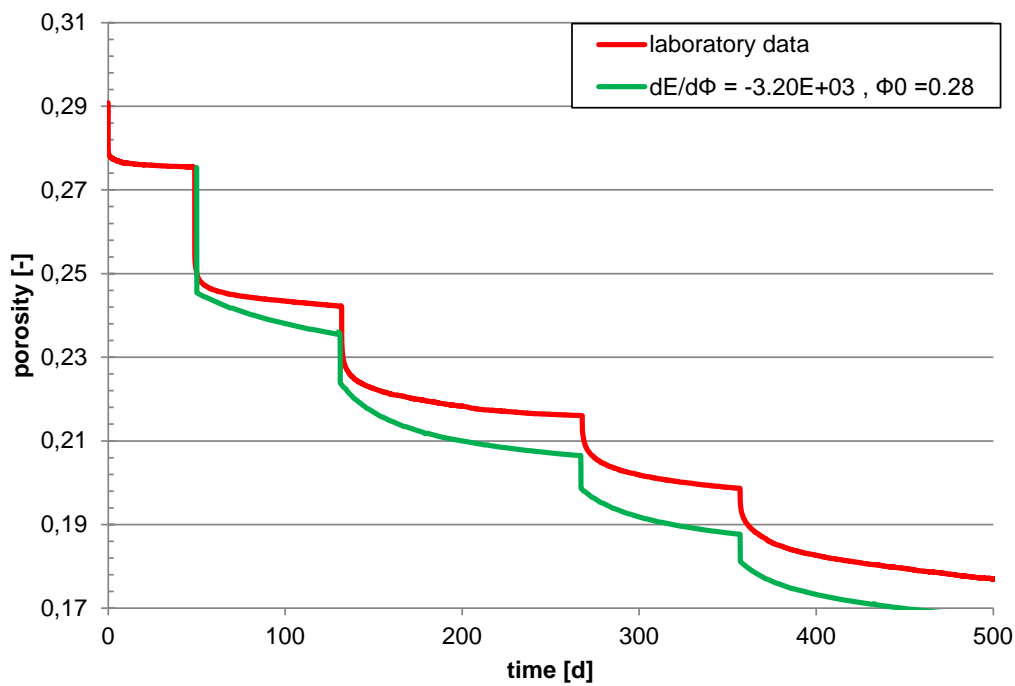
Fig. 3.17   Porosity evolution with time, variation **$dE/d\Phi = -3.20E+03$ MPa and $\Phi_0=0.28$**

Here you can see that the expectation was wrong. The curve is not approximated that good. The two parameters together are overestimated. Next $dE/d\Phi$ should be varied one more time to 4.00E+03 MPa.
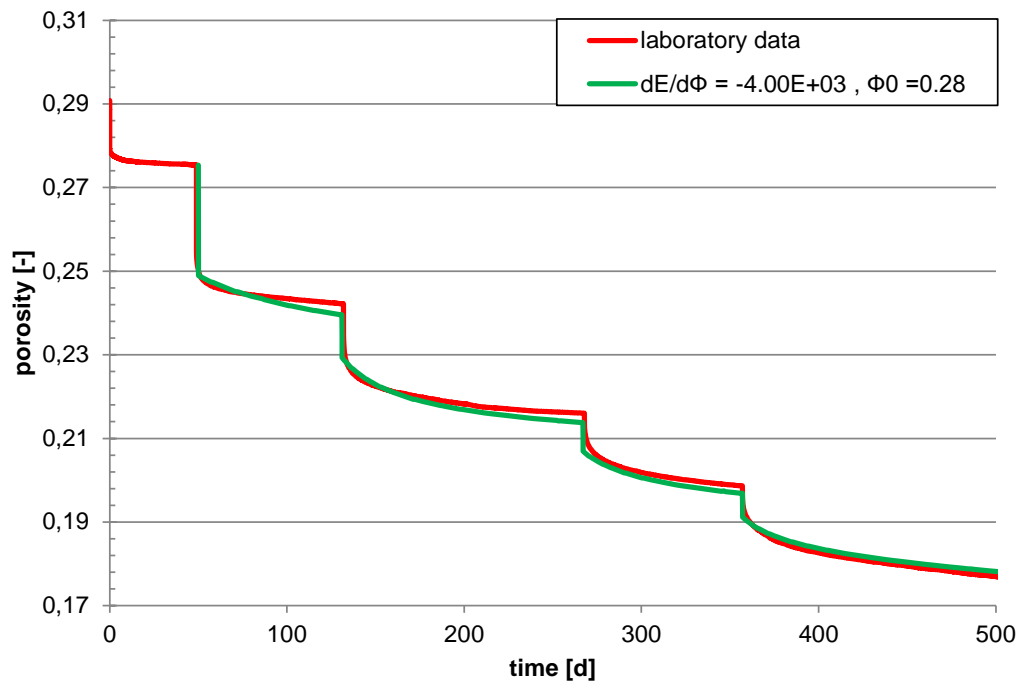
Fig. 3.18 Porosity evolution with time, variation **dE/dΦ= - 4.00E+03 and Φ_0=0.28**

This graph approximates the measured data very good. The parameter will be approached for the next phases.

In summary this parameter were varied:

- D from 1.00E+05 to 1.00E+04 [MPa]
- Γ_0 from 7.00E-04 to 7.00E-05 [s^{-1}]
- A_A from 2.08E-06 to 2.08E-08 [$s^{-1}MPa^{-n}$]
- dE/dΦ from -4.50E+03 to -4.00E+03 [MPa]
- Φ_0 from 0.30 to 0.28 [-]

3.3.3   Parameter variation thermal phase

In the mechanical phase the following laws were used:

- Linear Elasticity

In the thermal phase the following law was used:

- Linear Elasticity – Temperature and Suction

with the following parameters:

- a_s = Swelling coefficient for changes in suction
- b_s = Linear thermal expansion coefficient for the medium

The parameter that is varied is the linear thermal expansion coefficient for the medium.

The given value was b_s = 4.20E-05 °C^{-1}. To see how the parameter influences the graph the first two variations were b_s = 4.20E-06 °C^{-1} and b_s = 4.20E-04 °C^{-1}.

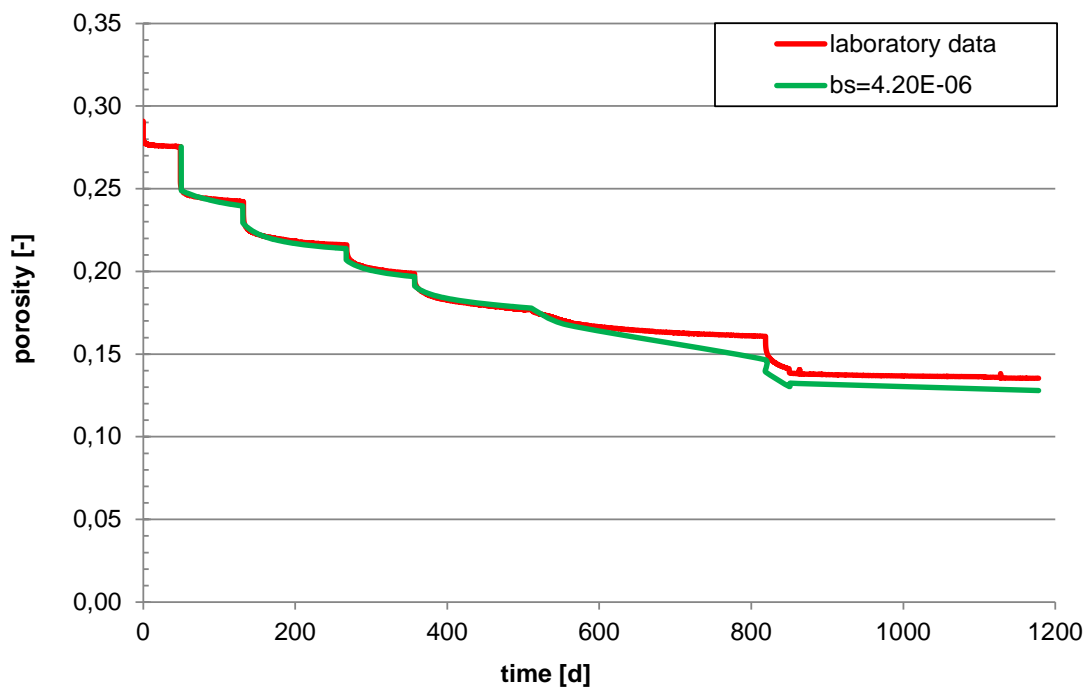In the following you can see that both graphs are not pretty good.

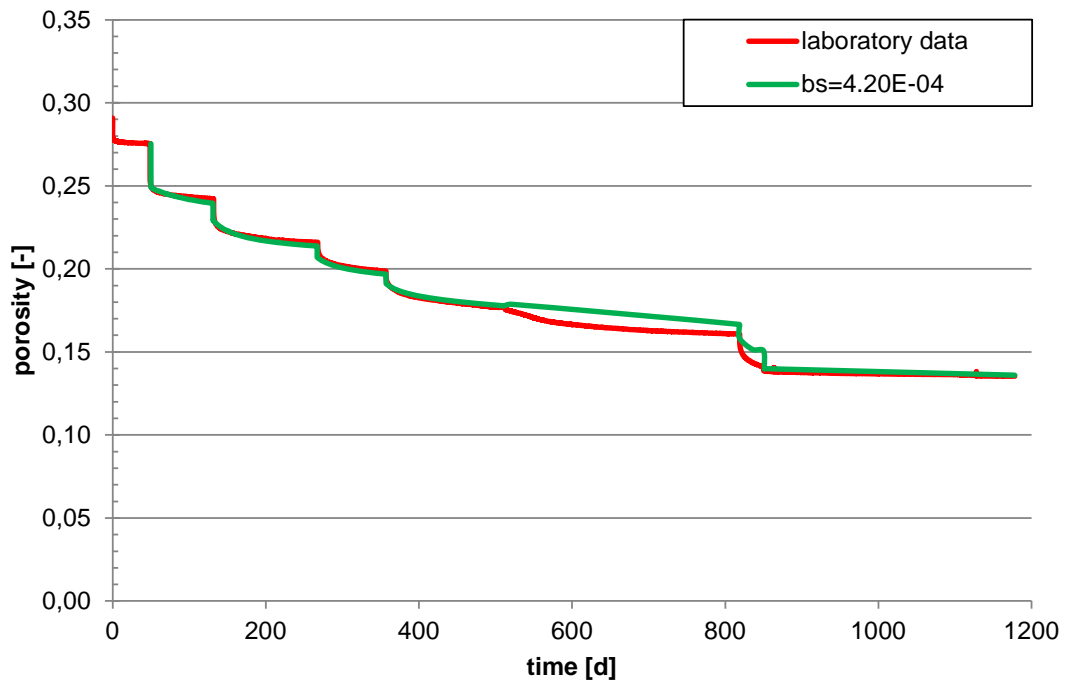**Fig. 3.19**   Porosity evolution with time, variation **b_s=4.20E-06 °C^{-1}**

Fig. 3.20 Porosity evolution with time, variation $b_s=4.20E{-}04\ °C^{-1}$

The decision was to take the second graph as a base and to reduce the parameter. The best approximation was with a parameter at about 2.90E-04.
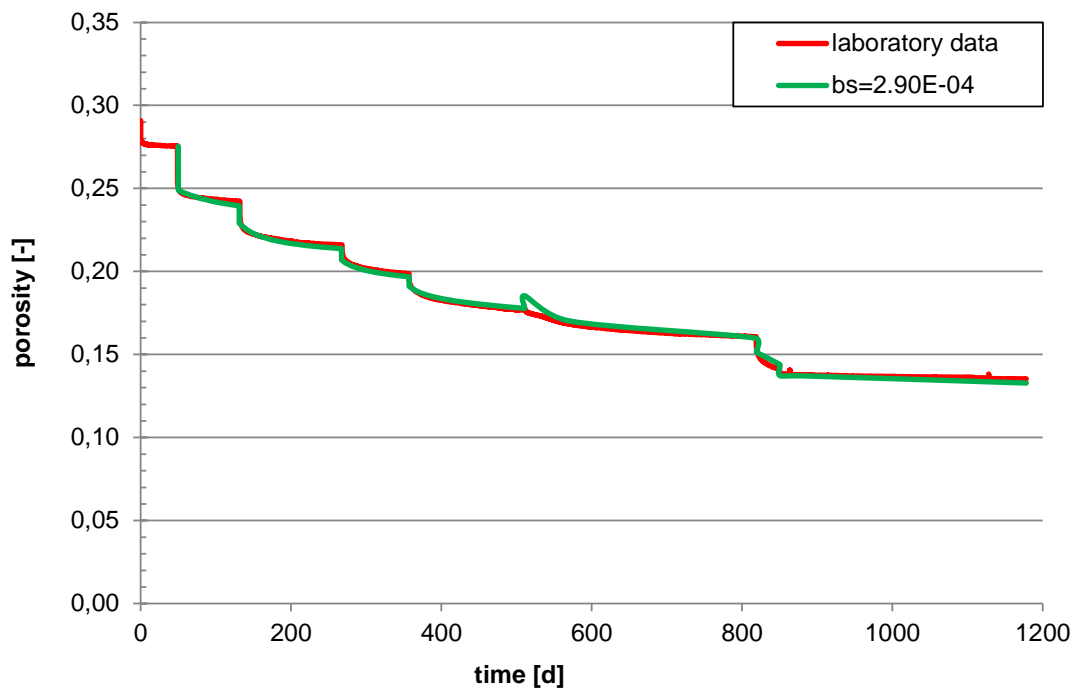

Fig. 3.21 Porosity evolution with time, variation $b_s=2.90E{-}06\ °C^{-1}$

The parameter b_s = 2.90E-04 °C^{-1} was adopted for the next steps.

3.3.4 Parameter variation hydraulic phase –*Initial dry sample*

The sample in the laboratory experiment was initially dry. Then brine was added to the sample in this phase.

To get a hydraulic component in CODE_BRIGHT the program uses the law:

- Viscoelasticity for saline materials.

The following parameter could be varied:

- d_0 = grain size
- A_B = pre-exponential parameter
- Q_B = activation energy

The decision was to vary the pre-exponential parameter at first and then vary the grain size.

Variation of the pre-exponential parameter A_B

The initial value was A_B = 1.00E-14 s^{-1}MPa^{-1}m^3 which was varied to A_B = 6.00E-13 s^{-1}MPa^{-1}m^3 in the report GRS-288. Because of the convergence the parameter was reduced to A_B = 6.00E-12 s^{-1}MPa^{-1}m^3.
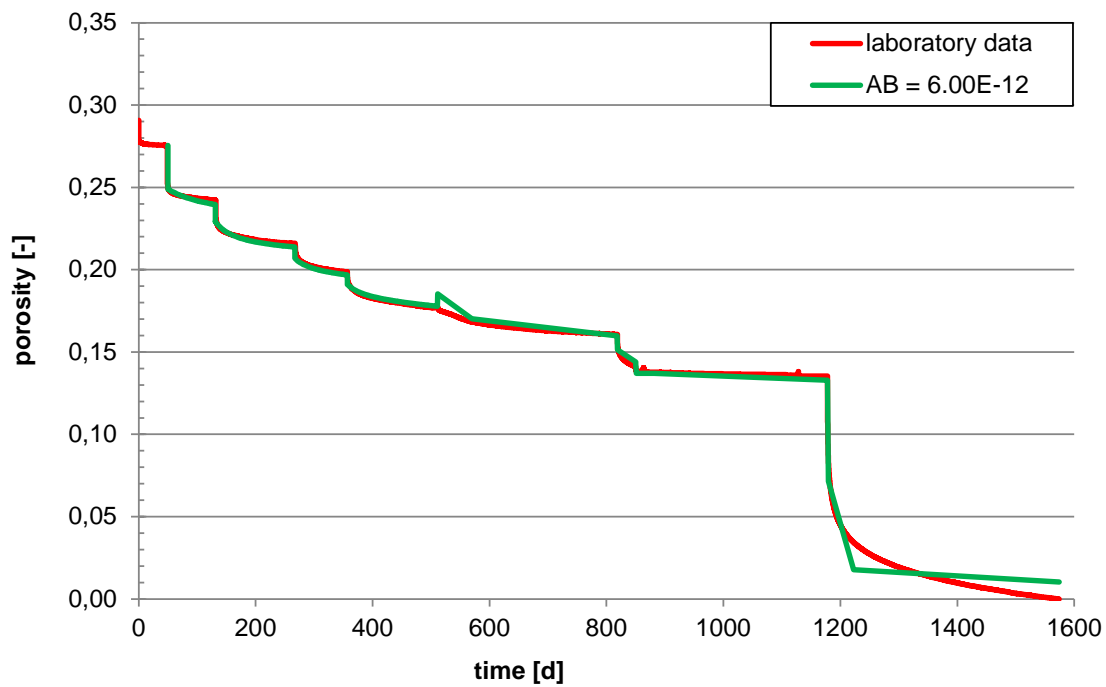
Fig. 3.22 Porosity evolution with time, variation $A_B = 6.00E\text{-}12 \ s^{-1}MPa^{-1}m^3$

The curve looks nearly perfect. But the claim is to get a better approximated curve in the time between 1200 days and 1600 days. To get an overview how the grain size effects the curve next this parameter will be varied.

Variation of the grain size

How mentioned an overview should be help to understand the behaviour of the modelling. The initial value was 1.50E-04 m which was raised up by GRS-288 to 4.00E-04 m. In dependence the first two variations were $d_0 = 4.00E\text{-}03$ m and $d_0 = 4.00E\text{-}05$ m.
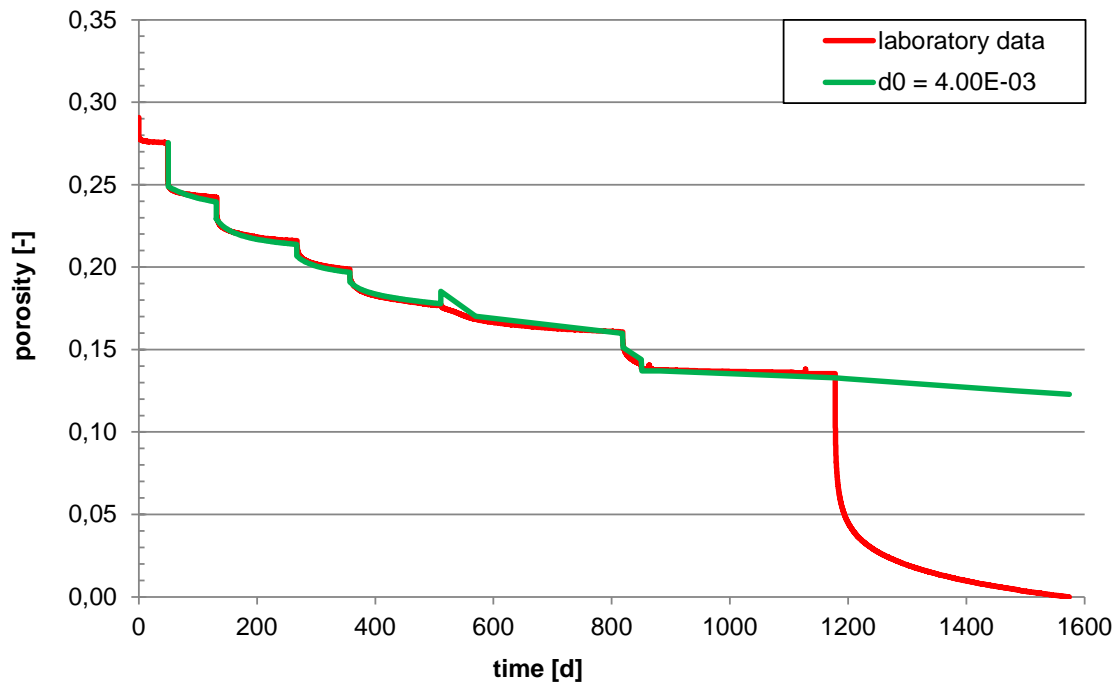
Fig. 3.23   Porosity evolution with time, variation **d0 = 4.00E-03 m**
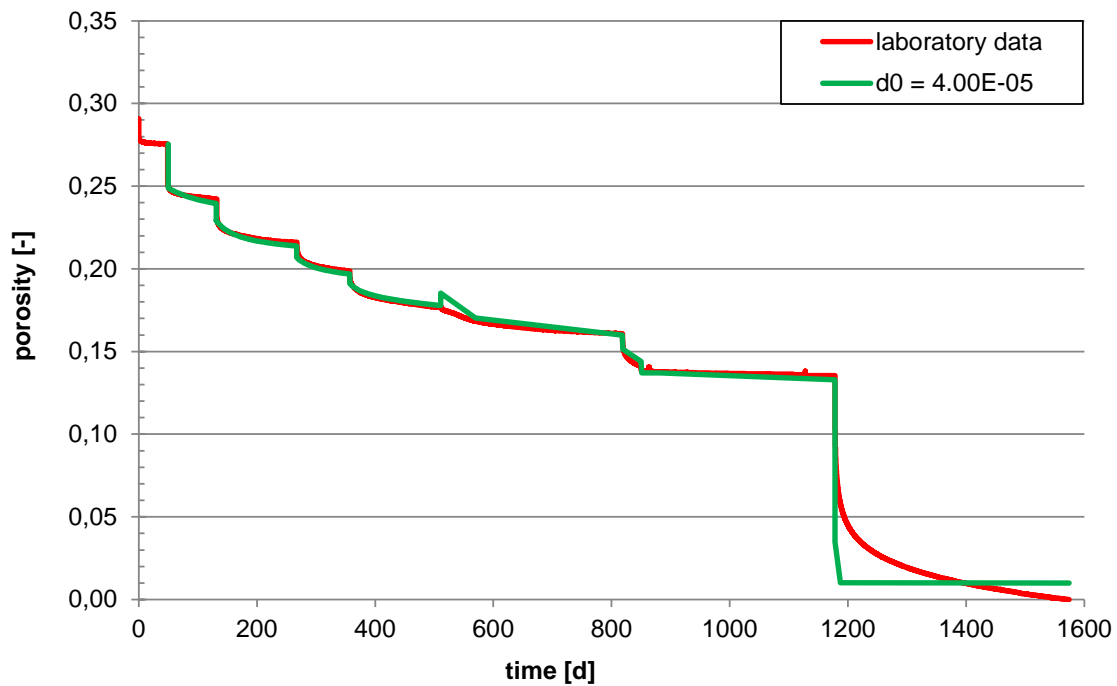

Fig. 3.24   Porosity evolution with time, variation **d0 = 4.00E-05 m**

It is to be seen that both of them are not good. Conspicuous are the radical fluctuations in the variation.

One last variation of the grain size was to set d_0 to 9.00E-04 m. Here the falling gradient in the time of 1200 days to 1600 days approaches to the measured graph.

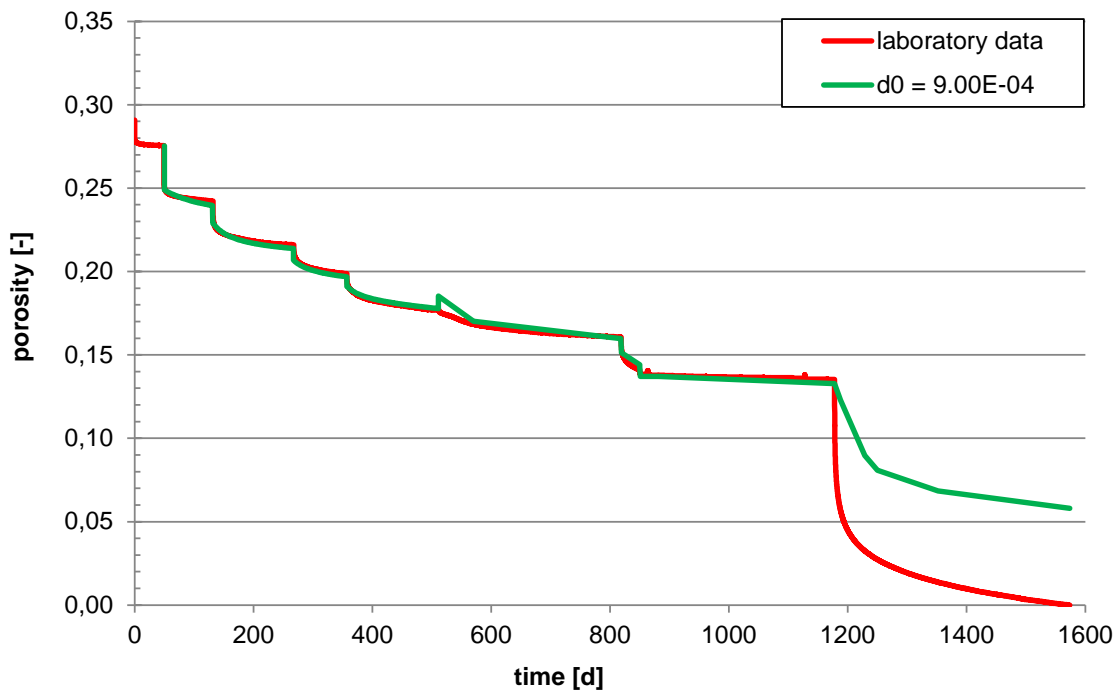**Fig. 3.25**   Porosity evolution with time, variation **d0 = 9.00E-04 m**

Variation of the pre-exponential parameter and the grain size

Because of the extreme fluctuations in the variation, we wanted to have a look how the two parameters influence themselves. The first parameters which were chosen are A_B = 6.00E-12 $s^{-1}MPa^{-1}m^3$ and d_0 = 9.00E-04 m.
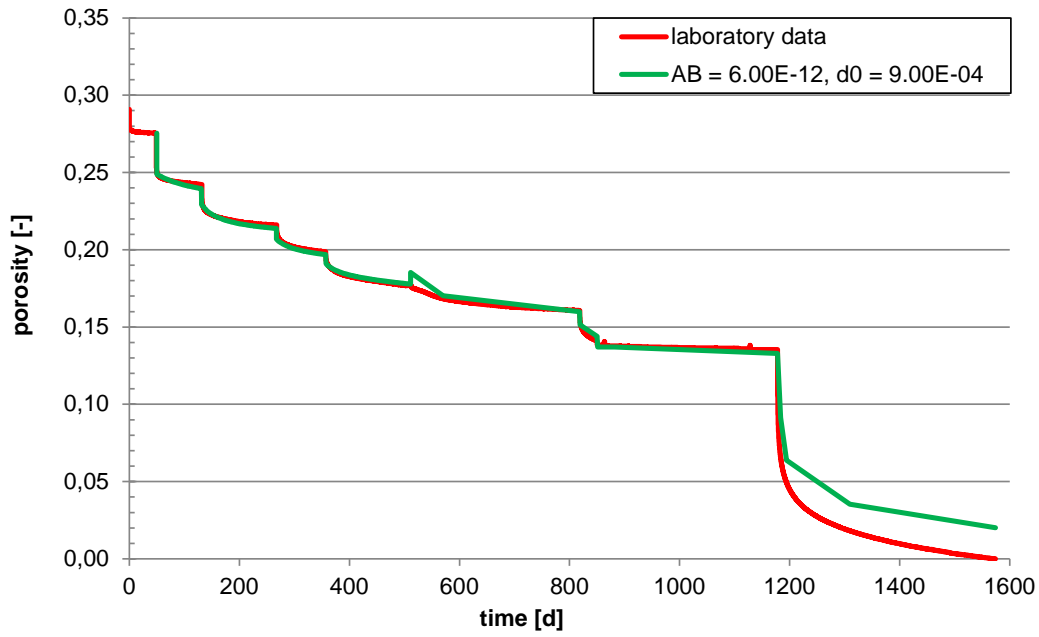
Fig. 3.26 Porosity evolution with time, variation **A$_B$ = 6.00E-12 s^{-1}MPa^{-1}m^3 and d$_0$ = 9.00E-04 m**

It is to be seen that the grain size has a big influence on the pre-exponential parameter. In the best approximation A$_B$ = 4.00E-11 s^{-1}MPa^{-1}m^3 and d$_0$ = 9.00E-04 m were used.
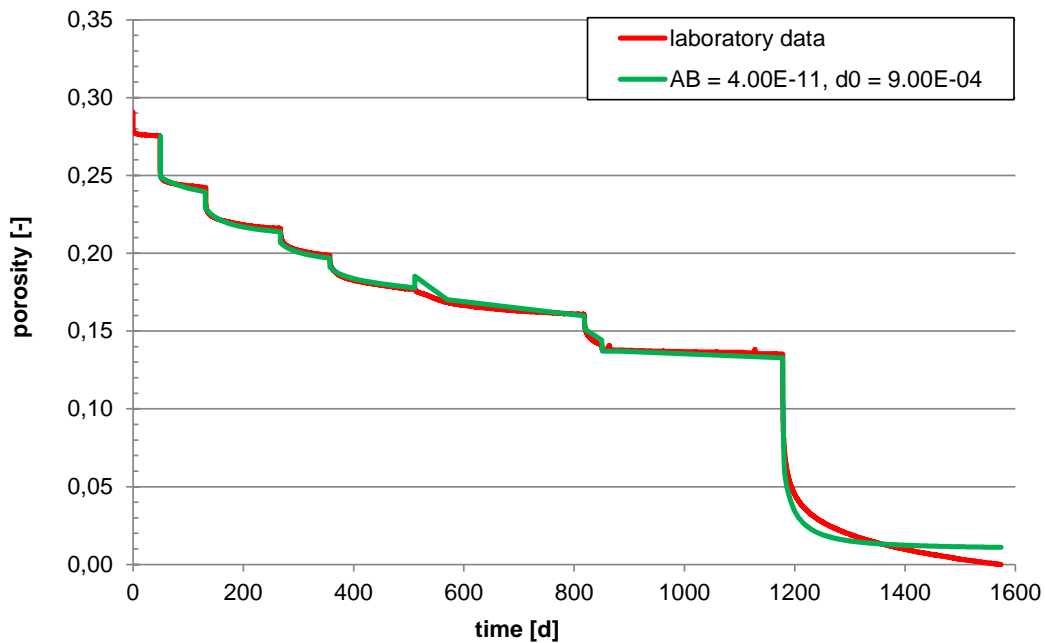
Fig. 3.27 Porosity evolution with time, variation **A$_B$ = 4.00E-11 s^{-1}MPa^{-1}m^3 and d0 = 9.00E-04 m**

3.3.5 Parameter variation hydraulic phase - *Sample with initial moisture of 1.0 %*

To prove the implemented FADT model the behaviour of a sample with initial moisture of 1.0 % should be modelled.

The boundary conditions of the numerical simulation are the same as mentioned in the beginning. The difference is that the FADT law affects the modelling in all intervals.

In the first modelling the parameter of GRS (2016) are used. GRS (2016) are the parameter found out in the prevenient variation. In result the modelled behaviour is much too soft. This is to be seen in the next Fig. 3.28.

The used parameters are adequate for the modelling of an initially dry curve, but not for the modelling of an initially moisture.

In the next simulations the parameters of GRS-254 and GRS-288 were used.
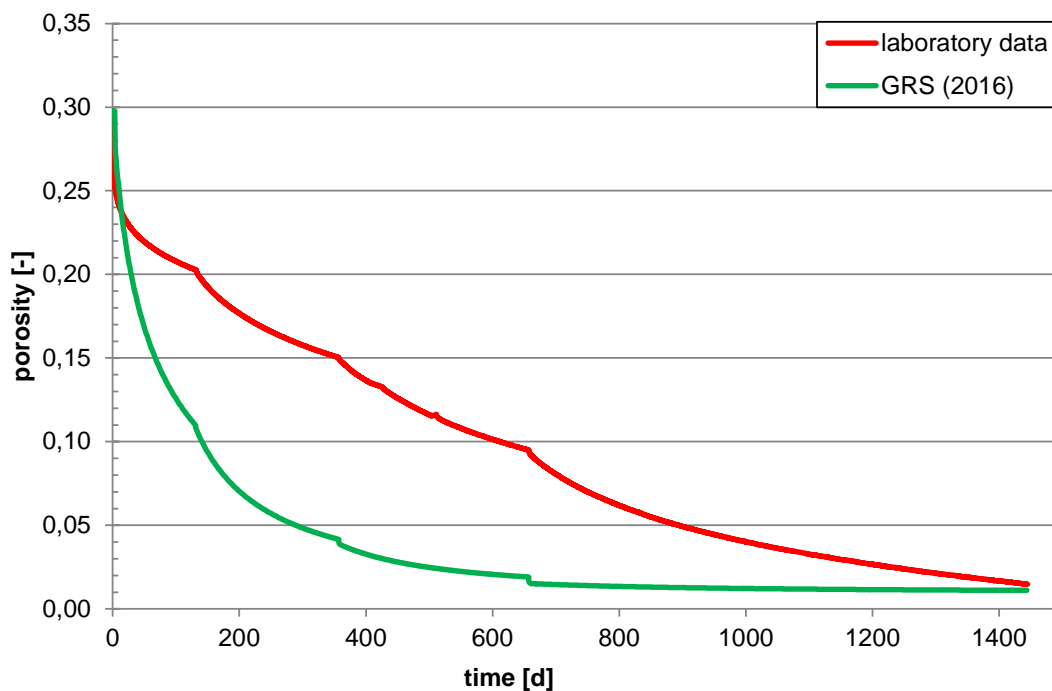

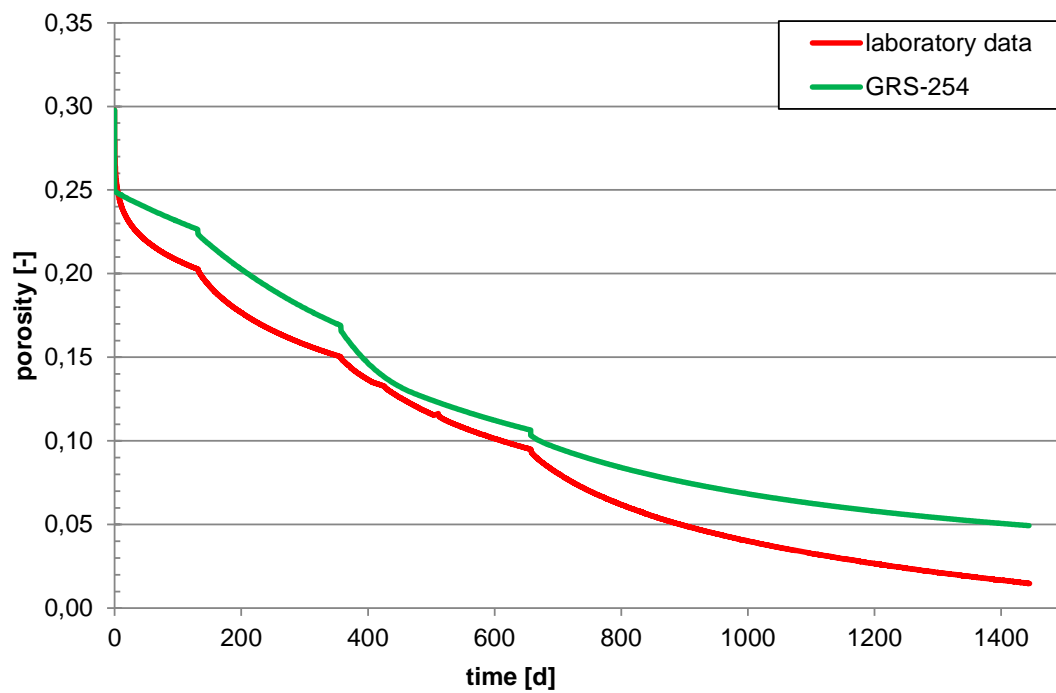**Fig. 3.28**   Porosity evolution with time, variation **GRS 2016**

Fig. 3.29   Porosity evolution with time, variation **GRS-254**
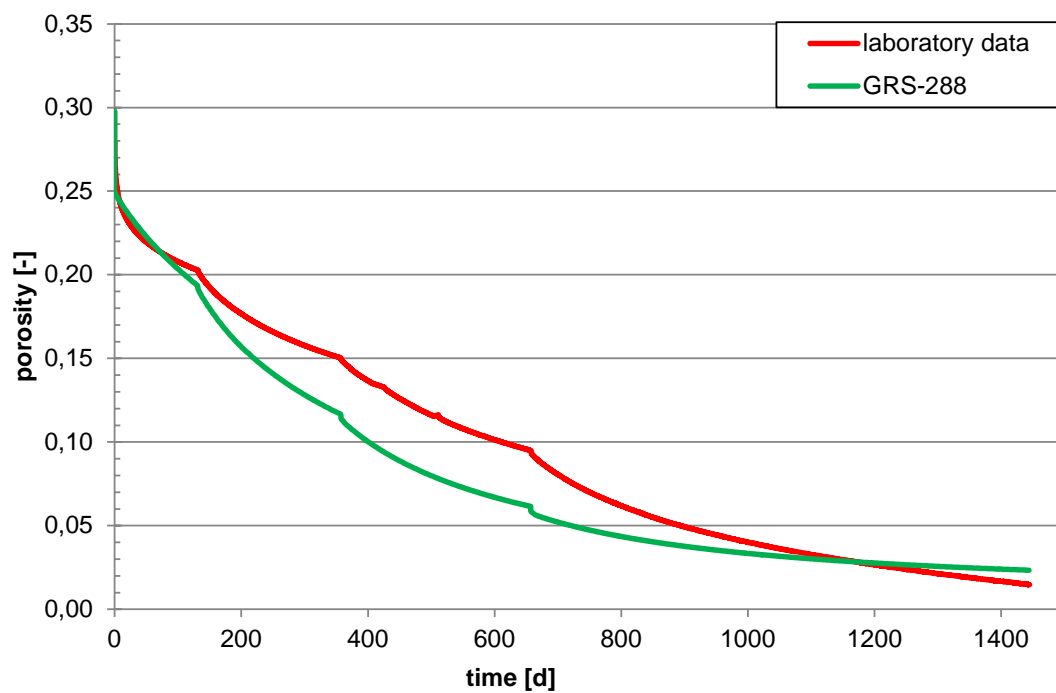

Fig. 3.30   Porosity evolution with time, variation **GRS-288**

It is conspicuous that the GRS-254 graph is above the laboratory data and the GRS-288 graph is below it. The presumption is that the final parameter must be in the range between the both parameters sets.

The parameters which could be varied are the activation energy A_B and the grain size d_0. Because of the closer position to the laboratory data, the GRS-288 graph was chosen to be the basis for this simulation.

So the parameters $d_0 = 4.00E\text{-}04$ and $A_B = 6.00E\text{-}13$ were firstly adopted. Now the activation energy A_B was set to $3.00E\text{-}13$ because it's the middle between the both GRS parameters.
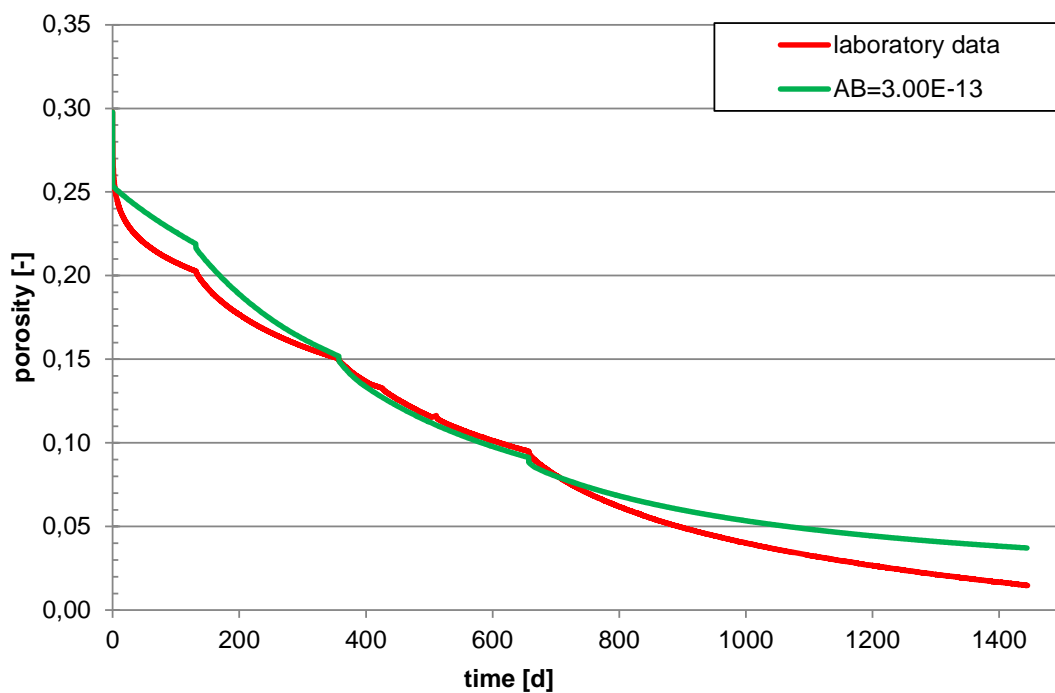

Fig. 3.31   Porosity evolution with time, variation **GRS (2016) after variation of parameter**

It was to be found that this is a good approximation to the laboratory data. $A_B = 3.00E\text{-}13$ would be permitted in the parameter data set.

3.4   THM-coupled modelling

In the previous chapter only a thermal-mechanical-coupled modelling was done. In the hydraulic phase the complete sample were flooded so that the saturation was 100%. But this is not the aim of a THM-coupling. In this chapter the real THM-modelling with a raising saturation will be done.

Therefore the sample with 1 % initial moisture will be used. The boundary conditions will be declared in the following table 3.1:To prove the implemented FADT model the behaviour of a sample with initial moisture.

Table 3.1: Initial conditions for the THM-coupled modelling

Surface conditions:	
Initial unknowns	P_l = - 1.0 MPa T = 29°C
Initial stress	$\sigma_x = \sigma_y = \sigma_z$ = - 0.1 MPa (atmospheric pressure)
Initial porosity	Φ_{salt} = 0.2977 Φ_{steel} = 0.1
Line conditions:	
Flux B.C.	Prescribed liquid pressure = -1.0 Gamma for liquid = 1e6

Furthermore there were only 8 intervals and 4 loading increments about the high of 1 MPa, 2 MPa, 4 MPa and 7 MPa. Another difference is that the temperature will be holding on 29 °C. This could be seen in the figure 37 in the previous chapter.

For a correct description of the hydraulic behaviour there were needed some more material parameters, e.g. to define the retention curve. The additional used material laws could be found in the appendix.

In the prevenient chapter the parameter set of GRS-288 fits the best for the coupled simulation. That is why these parameters are adopted for the next simulations. Furthermore the parameter for the activation energy A_B is set to 3.00E-13 s^{-1} MPa^{-1} m^3.
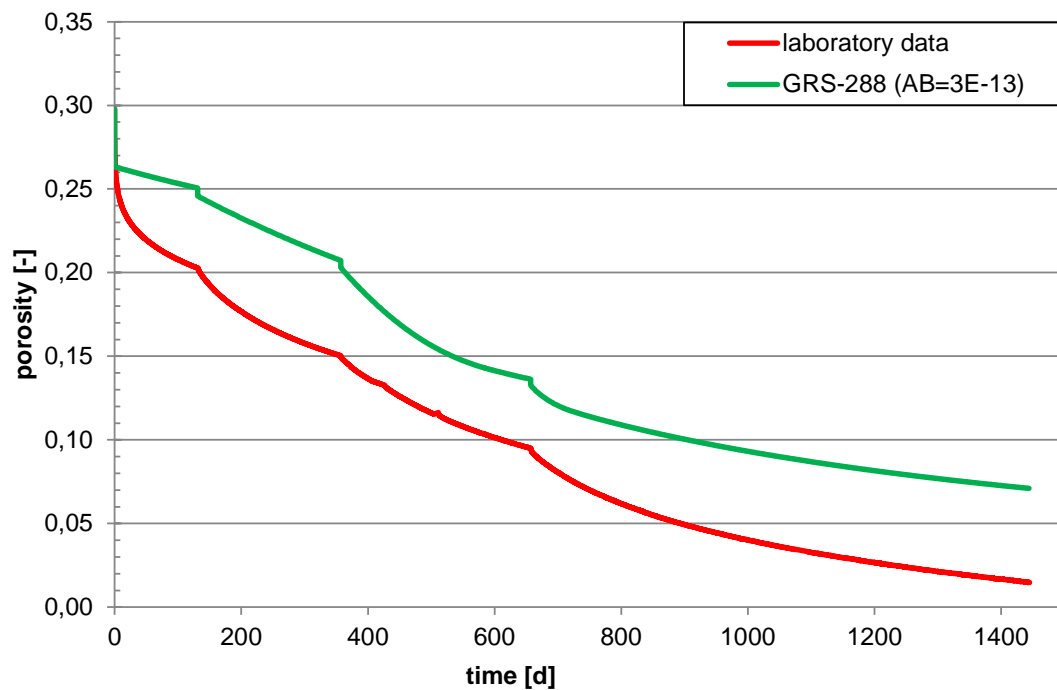
Fig. 3.32 Porosity evolution with time, variation **GRS-288 and A_B = 3.00E-13 s^{-1}MPa^{-1}m^3**

It is to be seen that the approximation is not good. Through the variation of the viscoelastic parameters the graph should be converges the laboratory data. The next graph shows the variation of the parameter A_B.

Fig. 3.33   Porosity evolution with time, variation A_B

Another variation was made with the reference porosity from the linear elasticity and the parameter A_B from the viscoelasticity law.
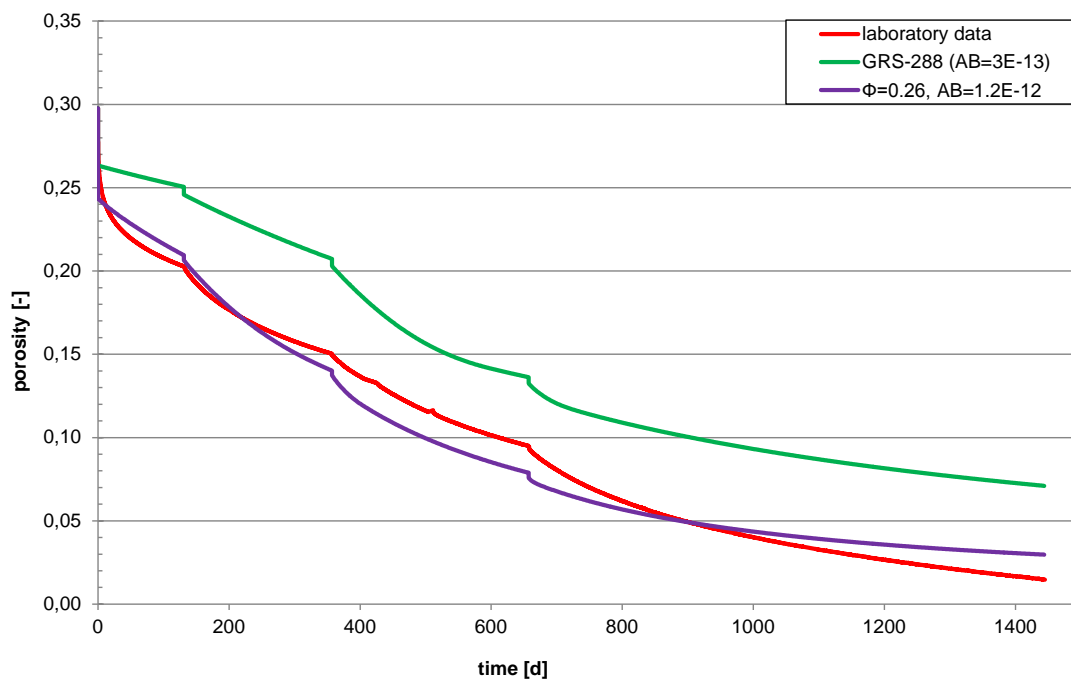
Fig. 3.34   Porosity evolution with time, variation A_B

4 Results

4.1 Back calculation using final data set

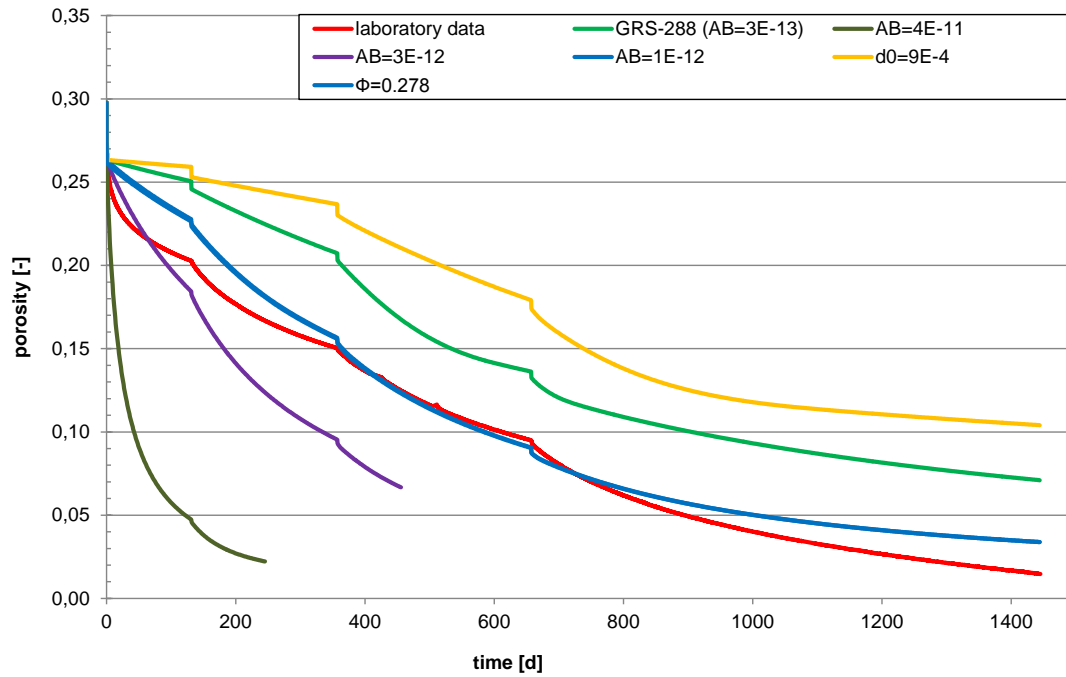In this section, the evolution of porosity in the sample centre as obtained in the calculations using different data sets is compared to experimental findings, Fig. 3.11. The sample-specific features that have been observed in lab (see chapter 2.4.2.5 and Appendix E) are met by the calculation results using parameter data set GRS (2016):

- The temperature increase to 60 °C causes a similar reaction in sample 1 as each stress increase, Fig. 3.13.
- The creep accelerating effect of the load increase to 18 MPa is cancelled at 850 days by reducing the temperature from 60 °C to 34 °C, Fig. 3.13.
- Flooding accelerated compaction in terms of the initial drop of porosity more than any other load change, Fig. 3.14.
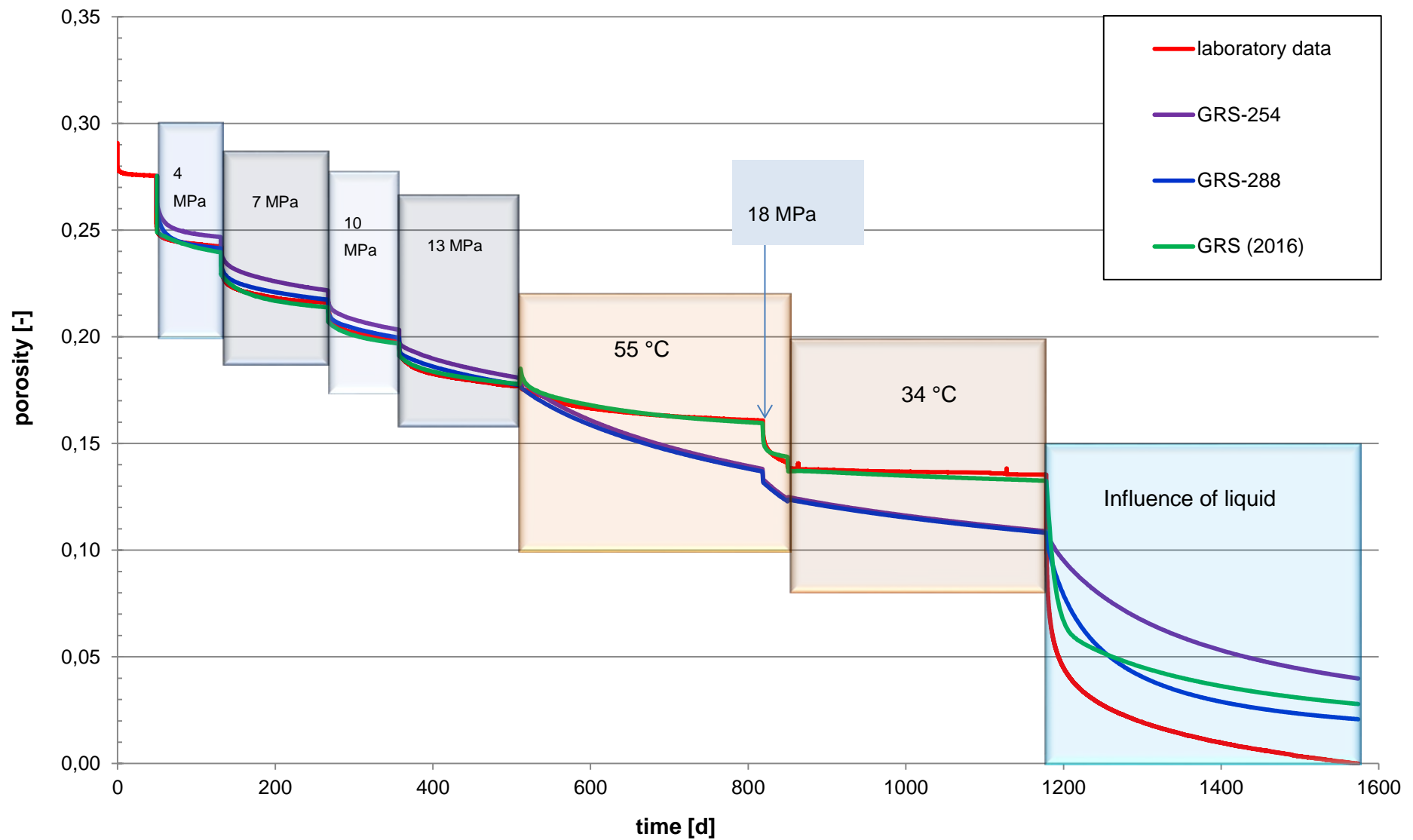
Fig. 4.1 Porosity evolution in the sample centre – comparison of different data sets

Legend:
- laboratory data
- GRS-254
- GRS-288
- GRS (2016)

Labels within figure: 4 MPa, 7 MPa, 10 MPa, 13 MPa, 18 MPa, 55 °C, 34 °C, Influence of liquid

Axes: porosity [-] (vertical), time [d] (horizontal)

46
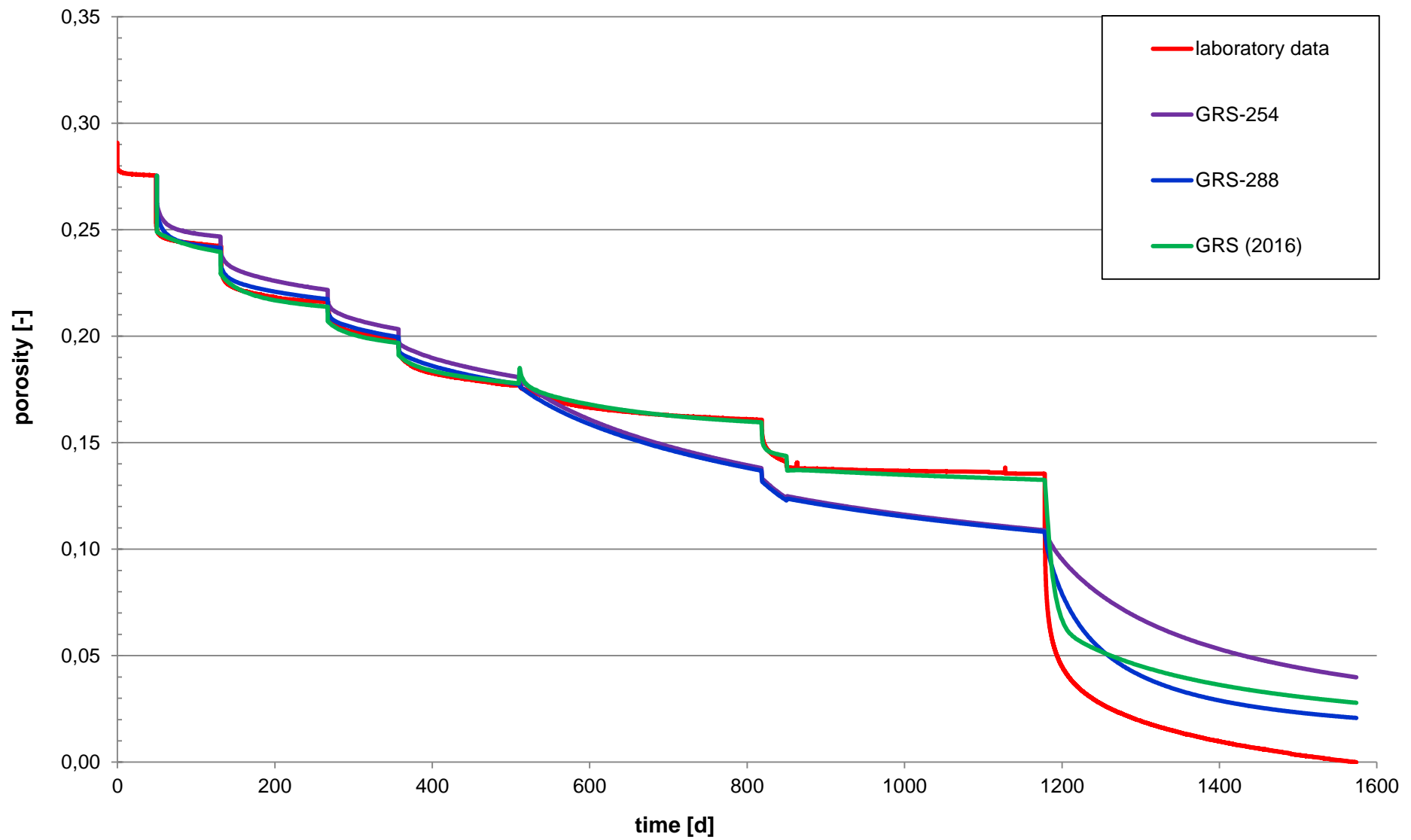
Fig. 4.2   Porosity evolution in the sample centre – comparison of different data sets

Fig. 4.3   Porosity evolution during the mechanical compaction phase – comparison of different data sets

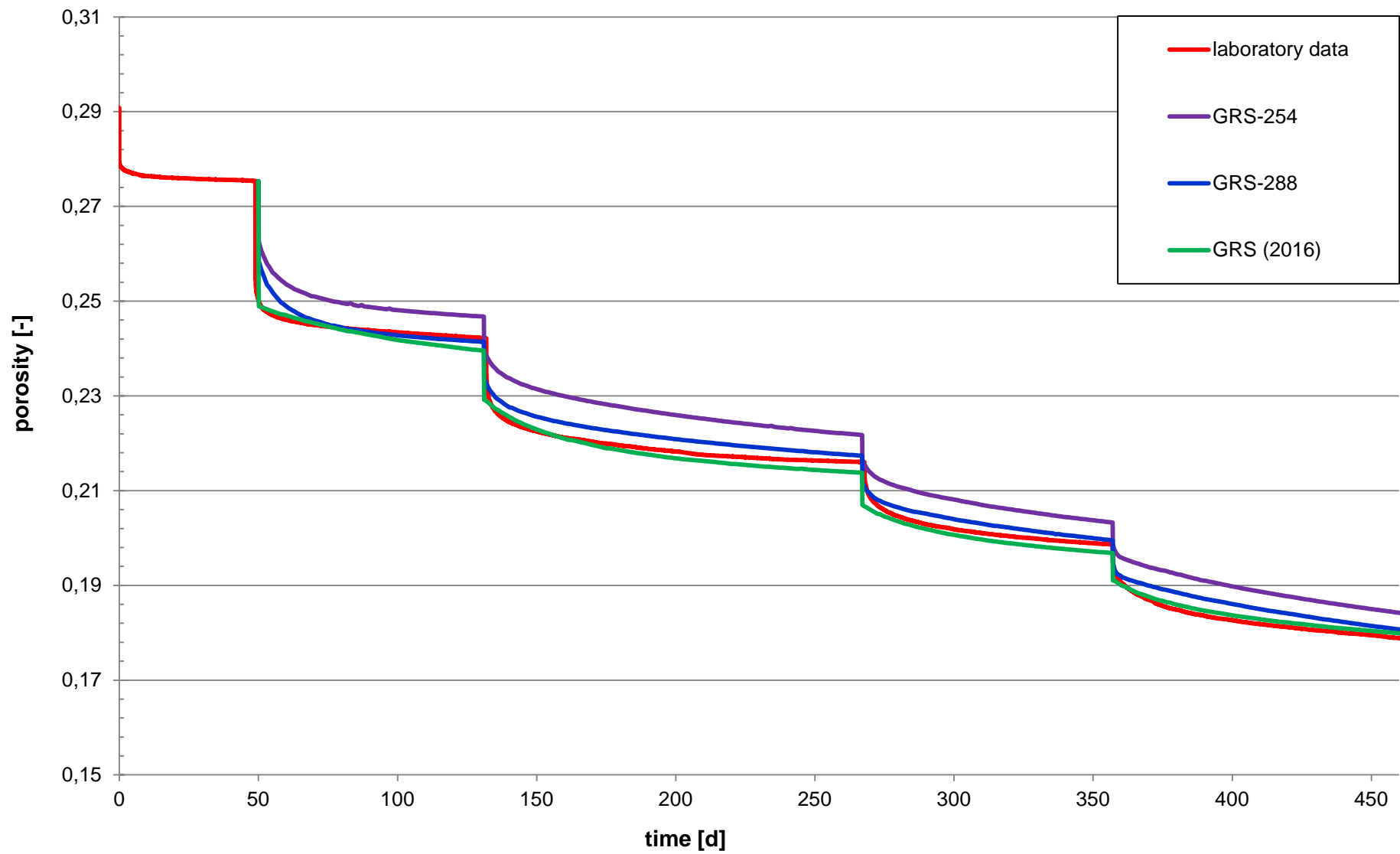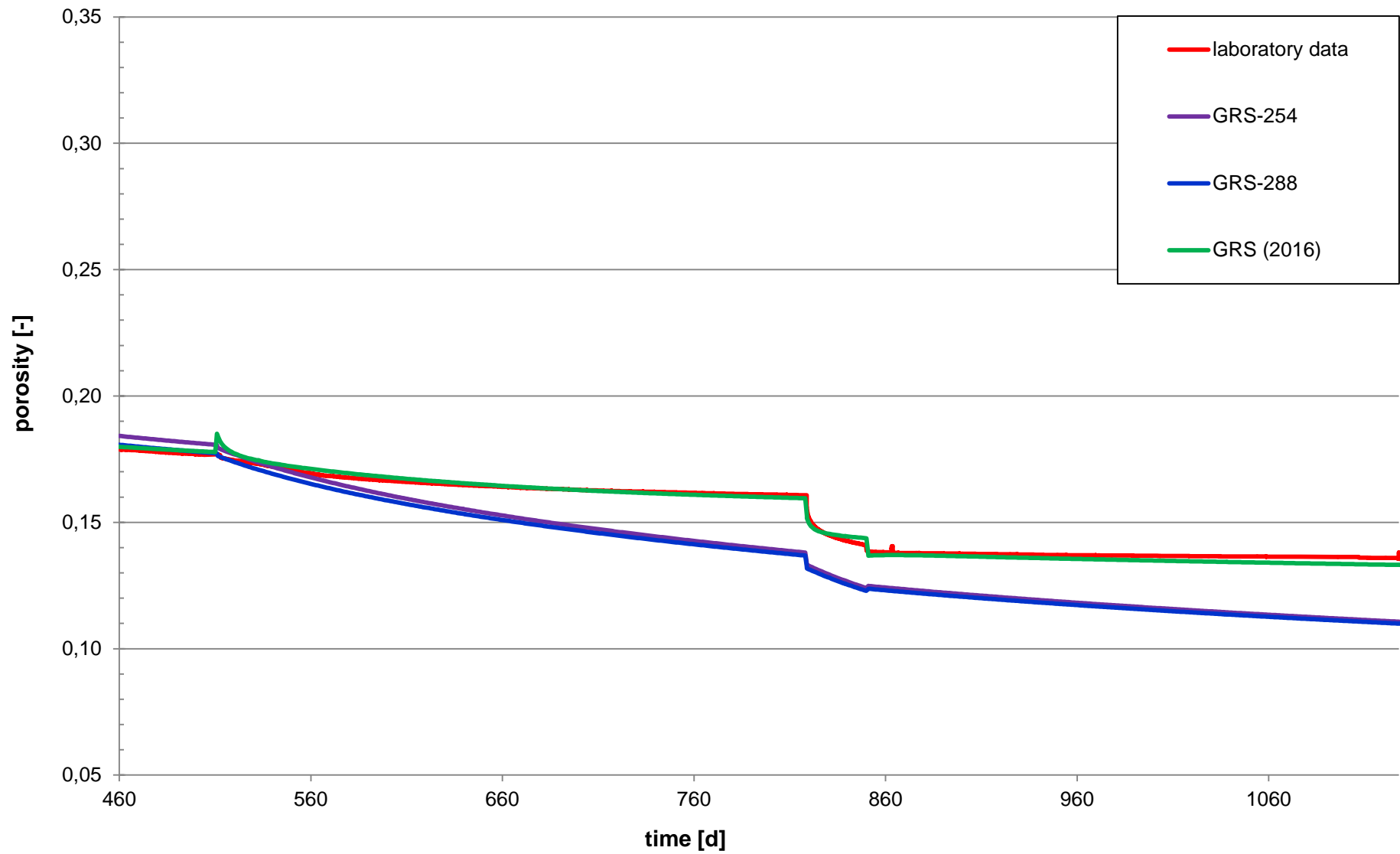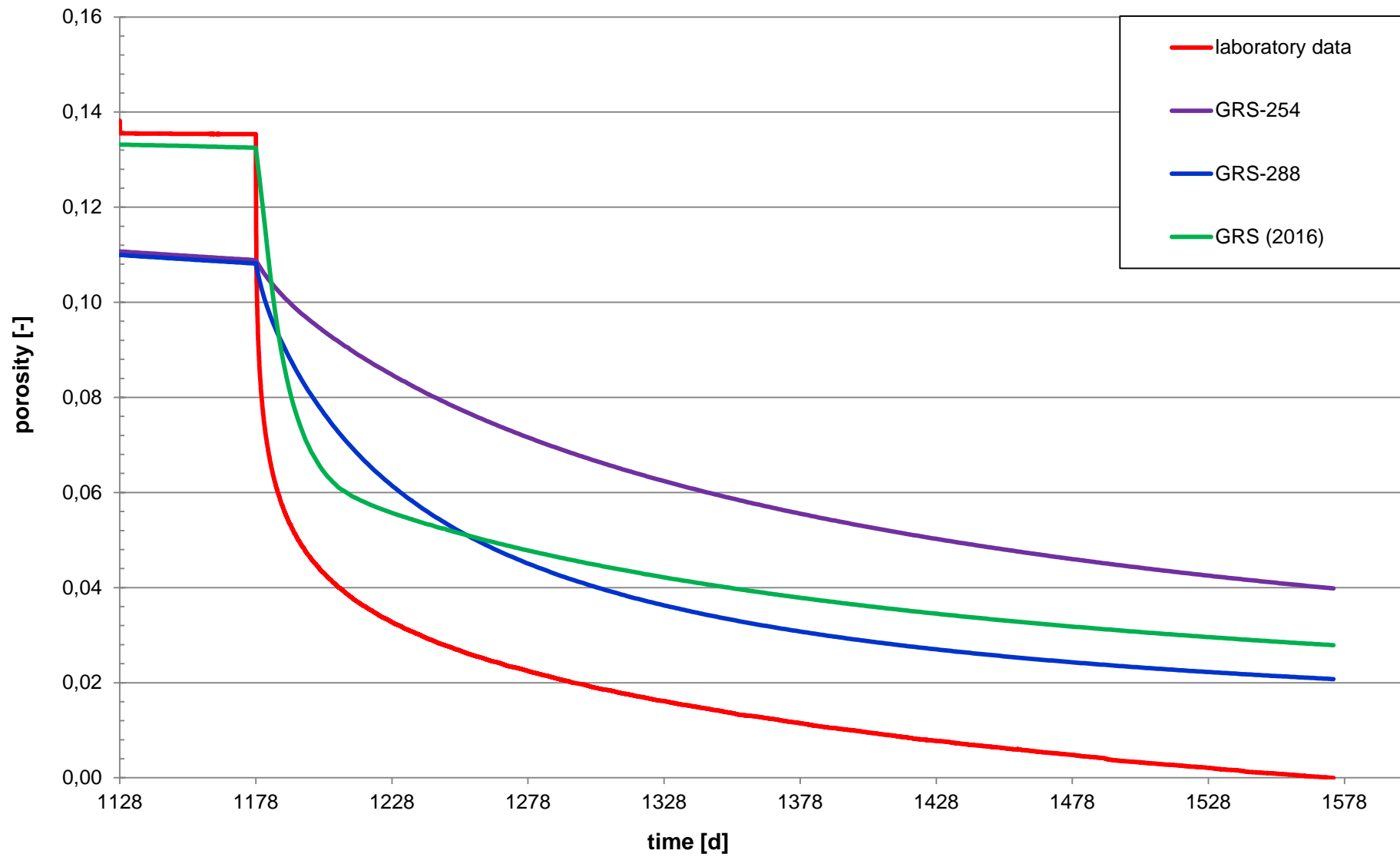**Fig. 4.4**   Porosity evolution during the thermal phase – comparison of different data sets

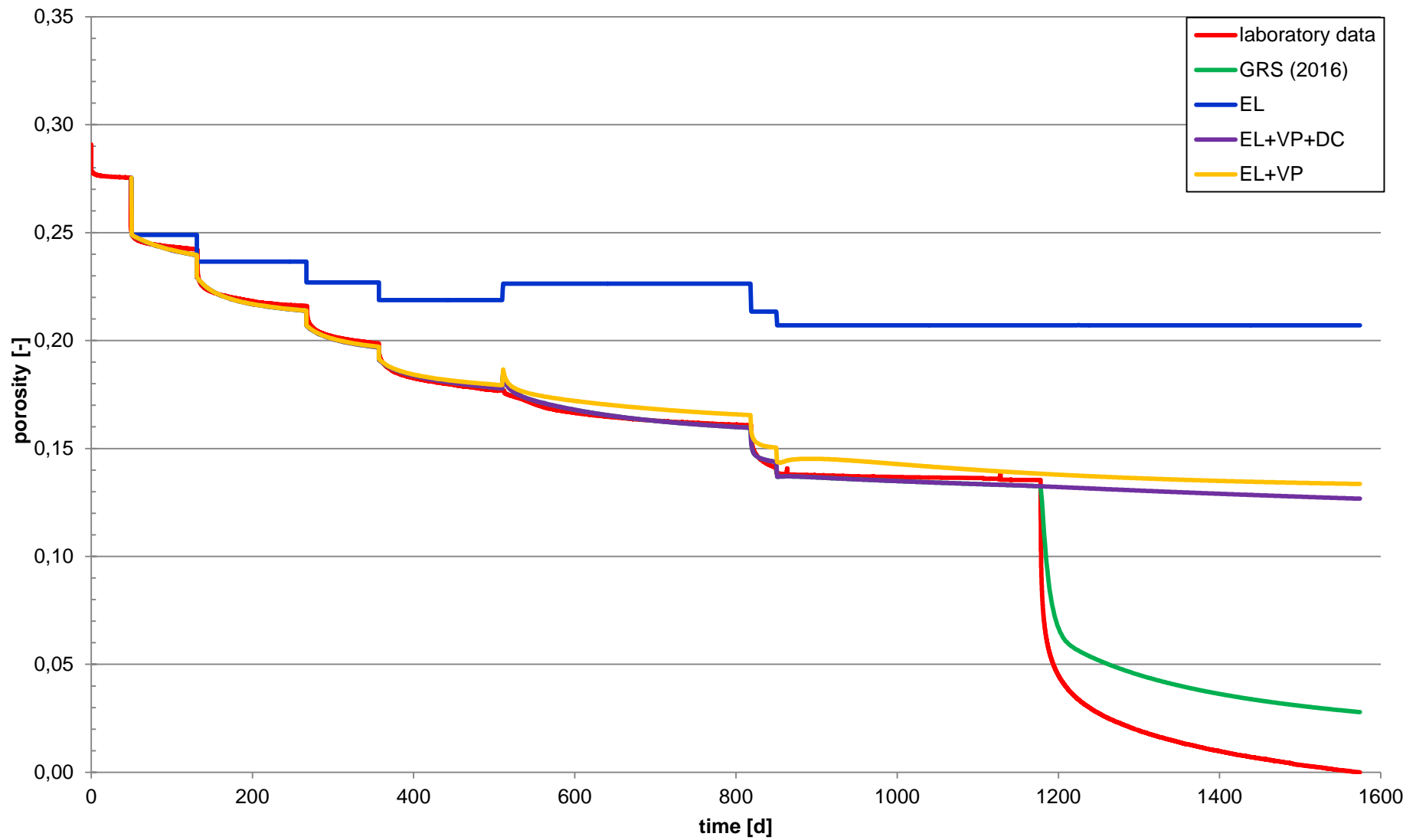**Fig. 4.5**   Porosity evolution due to brine injection – comparison of different data sets

Fig. 4.6　　　　Porosity evolution with time – Parts of the material models of GRS (2016**)**

4.2   Material parameter, GRS (2016)

Linear elasticity

E	1.0	MPa
$dE/d\Phi$	-4.00E+3	MPa
v	0.27	-
Φ_0	0.2977	-
Φ_{min}	0.1	-
E_{min}	0	MPa

Thermal expansion

b_s	2.90E-04	°C^{-1}

Fluid assisted diffusional transfer

d_0	4.00E-04	m
A_B	3.00E-13	s^{-1} MPa^{-1} m^3
Q_B	24530	J mol^{-1}

Dislocation creep

A_A	2.08E-08	s^{-1}MPa^{-n}
Q_A	5.40E+04	J mol^{-1}
n	5.00	-

Viscoplastic deformation behaviour of granular material

δ	10.00	-
Γ_0	7.00E-05	s^{-1}
Q	5.40E+04	J mol^{-1}
p_0	0.10	MPa
D	1.00E+04	MPa
l	4.00	-

Retention curve

P_0	0.01	MPa
σ_0	0.072	Nm^{-1}
λ	0.37	-
S_{rl}	0.01	-
S_{ls}	1	-

Instrinsic permeability

$(k_{11})_0$	1.00E-11	m^2
$(k_{22})_0$	1.00E-11	m^2
$(k_{33})_0$	1.00E-11	m^2
Φ_0	0.28	-
Φ_{min}	0.01	-

Liquid phase relative permeability

A	1	-
λ	3	-
S_{rl}	0.01	-
S_{ls}	1	-

Gas phase relative permeability

S_{rg}	0.99	-

Diffusive flux of vapour

D	5.9 E-6	$M^2 s^{-1} K^{-n} Pa$
N	2.3	-
τ_0	1	-
m	0	-

Diffusive flux of dissolved salt and air

D	1.1 E-4	$m^2 s^{-1}$
Q	24530	$J mol^{-1}$
τ	1	-

Conductive flux of heat

$(\lambda_{solid})_0$	6.1	$W mK^{-1}$
λ_{Gas}	1	$W mK^{-1}$
λ_{liq}	1	-
a_1	-2.43E-2	-
a_2	-5.8E-5	-
a_3	-5.5E-8	-

Solid phase properties

C_s	855	$J kg^{-1} K^{-1}$
ρ_s	2160	$kg m^{-3}$
α_s	4.2E-5	$°C^{-1}$
T_0	29	°C

Liquid phase properties

ρ_{lo}	1025	$kg m^{-3}$
β	4.5E-4	MPa^{-1}
α	-4.2E-4	$°C^{-1}$
γ	0.1	-

5   Conclusions

Different tests concerning dry compaction formed the basis for checking on the validity of the presently available material models. The idea behind this exercise was that a valid material model should correctly describe any of the compaction tests. However, this was not the case. None of the calibrated parameter sets could be transferred to another test with satisfying results. Using sets of intermediate parameter values led to the same result.

The simulations have shown that the application of the available material models on the long-term compaction tests leads to plausible and coherent results. Compaction of crushed backfill can in principle be modelled, both for the dry case and for a brine inflow, at constant or variable temperature.

While the numerical tools might be able to describe crushed salt compaction in principle, the understanding of the compaction tests in general and/or of the material models in particular is not sufficient to allow for reliable predictions at the time.

References

/COD 10/   CODE-BRIGHT User's Guide, Departament d'Enginyeria del Terreny, Cartogràfica i Geofisica, Universitat Politècnica de Catalunya (UPC), 2010.

/KRÖ 09/   Kröhn, K.-P., Stührenberg, D., Herklotz, M., Heemann, U., Lerch, C., Xie, M.: Restporosität und -permeabilität von kompaktierendem Salzgrus-Versatz; Projekt REPOPERM - Phase 1. Abschlussbericht, FKZ 02 E 10477 (BMWi), Gesellschaft für Anlagen- und Reaktorsicherheit (GRS) mbH, GRS-254, Köln, 2009.

GRS-288   Müller-Hoeppe, N., Breustedt, M., Wolf, J., Czaikowski, O., Wieczorek, K.: VSG: Integrität geotechnischer Barrieren - Teil 2 Vertiefte Nachweisführung (AP 9.2) **Vertiefte** Nachweisführung. FKZ UM10R03200, (BMU), Bericht GRS-288, GRS Braunschweig, 2012.